

AUS Repository

Enhanced Antimicrobial and Biofilm-Disrupting Properties of Gallium-Doped Carbon Dots

Item Type	Article;Peer-Reviewed;Published version
Authors	Radha, Remya;Fawad, Ahmad;Ravindran, Sreeshna;Boltaev, Ganjaboy;Philip, Sachin;Al-Sayah, Mohammad
Citation	Remya Radha, Ahmad Fawad, Sreeshna Ravindran, Ganjaboy Boltaev, Sachin Philip, and Mohammad H. Al-Sayah. "Enhanced Antimicrobial and Biofilm-Disrupting Properties of Gallium-Doped Carbon Dots" ACS Omega 2025 10 (25), 27559-27574, DOI: 10.1021/acsomega.5c03575
DOI	10.1021/acsomega.5c03575
Publisher	American Chemical Society
Download date	2026-04-12 17:03:44
Link to Item	https://hdl.handle.net/11073/26293

Enhanced Antimicrobial and Biofilm-Disrupting Properties of Gallium-Doped Carbon Dots

Remya Radha, Ahmad Fawad, Sreeshna Ravindran, Ganjaboy Boltaev, Sachin Philip, and Mohammad H. Al-Sayah*



Cite This: <https://doi.org/10.1021/acsomega.5c03575>



Read Online

ACCESS |



Metrics & More

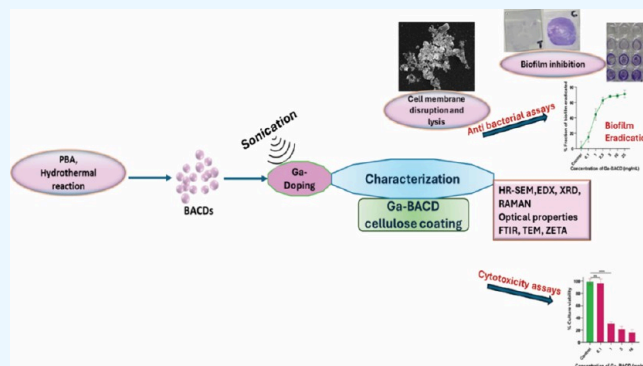


Article Recommendations



Supporting Information

ABSTRACT: Antibiotic resistance continues to be a global health threat caused by microbial biofilms, yet carbon dots (CDs) offer a promising countermeasure. Doping CDs with metals or nonmetals further enhances their properties while maintaining biocompatibility. This work reports the sonochemical synthesis of gallium-boronic acid carbon dots (Ga-BACDs) under conditions (20 kHz, 2000 W, 60% amplitude, 60 °C, and 60 min), achieving significant gallium incorporation. Ultraviolet–visible and fluorescence analyses reveal characteristic CD absorbance peaks at 286 and 355 nm and strong emission at 397–400 nm. Fourier transform infrared spectral changes on Ga-BACDs suggest successful incorporation of gallium and confirm Ga–H/Ga–O–C (2000–2600 cm^{-1}) and Ga–O/Ga–O–Ga (400–700 cm^{-1}) vibrations. X-ray diffraction and Raman spectroscopy data indicate the retention of the amorphous carbon framework with enhanced local ordering. High-resolution scanning electron microscopy (HR-SEM) and high-resolution transmission electron microscopy images demonstrate morphological alterations compared to BACDs with a particle mean diameter of 8.6 ± 4.1 nm. The gallium doping in Ga-BACDs was quantified as 3.66 ppm by using inductively coupled plasma–atomic emission spectroscopy. X-ray photoelectron spectroscopy results indicated that Ga is chemically integrated inside the carbon dot framework. The zeta potential shifts from -32.5 mV (BACDs) to -23.3 mV (Ga-BACDs), evidencing surface charge modulation. The antimicrobial activity of Ga-BACDs was tested against Gram-positive (*Staphylococcus epidermidis*) and Gram-negative (*Escherichia coli*) bacterial strains; the presence of gallium contributed to improved bioactivity at 37 °C. HR-SEM images of Ga-BACD-treated bacteria presented significant structural damage, membrane rupture, and surface irregularities. Ga-BACDs inhibited biofilm formation at concentrations as low as 2.5 mg/mL and efficiently eradicated preformed biofilms, highlighting their promise for preventing biofilm-associated infections. MTT assays on normal human brain cells confirm the biocompatibility of Ga-BACD-coated cellulose discs and CD solution (0.1 mg/mL), supporting the safe use of Ga-BACD-modified fibers. Overall, our findings highlight Ga-BACDs as metal-doped carbon nanoparticles, with strong potential for novel antibacterial treatments.



1. INTRODUCTION

Bacterial biofilms are well-structured bacterial communities enclosed in a self-generated extracellular matrix of proteins, lipids, and primarily polysaccharides.^{1–3} This polysaccharide matrix is essential for biofilm formation, providing essential functions such as adhesion, structural integrity, and protection against external threats.^{4,5} The polysaccharide component acts as a molecular glue, facilitating irreversible bacterial attachment to each other and surfaces, enabling the formation of robust biofilms.^{6,7} As the biofilm matures, bacteria within it produce extracellular polymeric substances (EPSs), further enhancing their structural complexity and resistance.^{3,8} The biofilm enables bacteria to form structured communities and enhances the bacterial cell-to-cell communication mechanism, known as quorum sensing (QS).^{9,10} Due to these factors, biofilm formation contributes to the bacteria's high resistance to

antibiotics and immune responses, which poses significant challenges in clinical settings, particularly on medical devices and chronic condition infections.^{11–14} The rise of antibiotic-resistant bacteria has increased the need for alternative therapeutic approaches to prevent or treat biofilm-associated infections, offering the potential to improve treatment outcomes for various infectious diseases.^{15,16}

Recent advancements in nanotechnology highlight the potential of carbon nanomaterials (NPs), particularly carbon

Received: April 18, 2025

Revised: June 2, 2025

Accepted: June 10, 2025

dots (CDs) and quantum dots.^{17,18} Their unique physicochemical characteristics, like the high surface area and tunable optical and fluorescence sensing properties with excellent biocompatibility, make them effective against a wide range of microbes and other pathogens.¹⁹ The nanoscale size of these particles enables penetration into microbial cells, causing damage through cytoplasmic leakage, the generation of reactive oxygen species (ROS), and genetic material fragmentation.²⁰ Moreover, their surface functionalization enhances antimicrobial effectiveness, making them a viable option for biofilm disruption.²¹ These NPs are even used in antibacterial coatings for implantable devices and medical materials, providing a protective antimicrobial layer, reducing the risk of bacterial colonization and biofilm formation on surfaces.²² By incorporating NPs into medical devices such as catheters, stents, and surgical implants, their antimicrobial properties enhance patient safety and promote faster healing, minimizing the need for long-term antibiotic treatments.^{23,24}

Studies on metal-doped nanoparticles have shown enhanced physicochemical properties, enabling their wide application in medicine and disease treatment.^{25–29} The antibacterial activity of metal-doped carbon quantum dots with metals Fe, Zn, Mn, Ni, and Co showed higher activity in Gram-negative *Escherichia coli* (*E. coli*) compared to Gram-positive *Staphylococcus aureus*, with the highest efficiency for Mn-doped particles.³⁰ Recent studies on copper-doped carbon dots addressed their antimicrobial properties, cancer photothermal therapy, optical bioimaging,^{31–33} particularly as a nanomouthwash for removing oral biofilms, wound healing, and teeth whitening, highlighting their potential in oral health management.²²

Gallium (Ga), a group IIIA metal, shares similarities with iron (Fe^{3+}) in terms of ionic charge, radius, and electronic configuration, allowing it to mimic iron in many biological processes.³⁴ Ga exhibits potent antimicrobial and antitumor activities by disrupting iron homeostasis in bacterial, fungal, and tumor cells.^{35–37} It interferes with ribonucleotide reductase, mitochondrial function, and iron transport proteins, making it a potent antimicrobial agent. However, since Ga^{3+} cannot replace Fe^{3+} as a cofactor in redox-dependent enzymes, it inhibits essential biological functions, such as iron metabolism, disrupting bacterial growth. This ability to exploit gallium's disruption of iron metabolism provides a promising strategy against a range of bacterial species.^{38,39}

Ga-based metal–organic frameworks (MOFs) have shown potential in combating bacterial infections.⁴⁰ Recent studies on gallium carboxymethyl cellulose indicate that Ga ions can disrupt the iron metabolism crucial for bacterial survival, inhibiting the growth of both planktonic and biofilm forms.⁴¹ Gallium nanoparticles (Ga NPs) have been shown to inhibit biofilm formation in *Pseudomonas aeruginosa* (*P. aeruginosa*) DFU53 and multidrug-resistant *Acinetobacter baumannii*.³⁷ Another study on gallium curcumin nanoparticles reported the effective antibacterial activity against the pathogenic bacterium *P. aeruginosa*.⁴² Additionally, increasing the Ga doping level in CDs has enhanced antimicrobial activity against *P. aeruginosa*, suggesting that Ga-CDs could be an effective new tool for bacterial infection treatment.³⁴

While gallium-based nanomaterials have been extensively studied for their antibacterial effects against various infections, research specifically focused on gallium-doped carbon dots (Ga-BACDs) remains limited. Biofilm-associated infections on implantable devices, such as vascular stents and biofilm formation on medical devices, continue to pose clinical

challenges due to biofilm resistance. There is a critical need for innovative antimicrobial strategies that are capable of effectively preventing bacterial colonization and eradicating biofilms. This study aims to synthesize and characterize Ga-doped bioactive carbon dots (Ga-BACDs) and their modified cellulose fibers, evaluating their antimicrobial activity and efficacy in disrupting microbial biofilms. By enhancing the intrinsic properties of carbon dots through gallium doping, this research aims to develop advanced nanomaterials for infection control in biomedical applications.

2. MATERIALS AND METHODS

2.1. Chemicals and Materials. The primary chemicals and materials used in this study include gallium (99.99%), phenylboronic acid (PBA), and phosphate-buffered saline tablet capsules, all of which were purchased from Sigma-Aldrich (Baden-Württemberg, Germany). Cellulose paper discs with a 7 mm diameter (Whatman filter paper (grade 1)) were used as the substrates for the attachment of the carbon dots.

2.1.1. Bacterial Cell Culture. The bacterial studies were performed using Gram-negative *Escherichia coli* (MicroKwik culture 15S065A) and Gram-positive *Staphylococcus epidermidis* (SE). Autoclaved tryptic soy broth (Millipore) and Mueller Hinton broth (Millipore) were used for culturing and bacterial assay experiments. All bacterial assays were conducted in 96-well microtiter plates (Corning, USA).

2.1.2. Animal Cell Culture. The biocompatibility of gallium–boronic acid carbon dots (Ga-BACD) was assessed by evaluating their toxicity in a normal human brain microvascular endothelial cell line (HBMEC). The cells were cultured and maintained in Dulbecco's modified Eagle medium (DMEM, Sigma-Aldrich), supplemented with 10% (v/v) fetal bovine serum (FBS, Sigma-Aldrich) and 10% (v/v) penicillin–streptomycin (Sigma-Aldrich) (containing 10,000 U/mL penicillin and 10 mg/mL streptomycin) before use. Additional reagents used included trypsin-EDTA solution (Sigma-Aldrich), Dulbecco's phosphate-buffered saline (Sigma-Aldrich), dimethyl sulfoxide (DMSO), and thiazolyl blue tetrazolium bromide (Sigma-Aldrich, USA). The experiments were conducted using 24- and 96-well tissue culture plates (Corning, USA).

2.2. Synthesis of Ga-BACDs. Ga-BACDs were synthesized by dispersion of gallium metal on boronic acid carbon dots (BACDs). BACD solution was synthesized via a hydrothermal reaction, following the method described in our previous studies.^{17,18} A solution of phenylboronic acid (100 mg/10 mL, pH 9.0) was prepared and subjected to thorough sonication and degassing under nitrogen gas for 30–40 min. The reaction was carried out in a hydrothermal reactor at 160 °C for 8 h, followed by centrifugation at 10,000 rpm for 15–20 min to separate the supernatant carbon dots.

Gallium doping was carried out on BACDs using an ultrasonic-assisted method.⁴³ A small gallium granule containing the BACD solution was placed in a glass or falcon tube. The tube was immersed in a 70 °C water bath setup, and the tip of an ultrasonic homogenizer (model LUHS-A20, frequency 20 kHz, ultrasonic power 2000 W, voltage 220 V/50 Hz, Labtron Equipment, UK) was positioned approximately 2 cm above the gallium (the sonication setup is shown in Figure S1). Once the gallium metal was completely melted, ultrasonication was performed for 60 min at a 60% amplitude to facilitate gallium dispersion and the formation of a gray suspension. The resulting mixture was centrifuged at 10,000 rpm for 30 min to separate solid particles. The gallium-doped BACD (Ga-BACD)

remained in the supernatant and was collected for further characterization and analysis.

The Ga-BACD solution was subjected to freeze-drying to obtain a powdered form, which was subsequently used for bacterial assays.

2.3. Ga-BACD Coating on Cellulose Paper Discs.

Whatman filter paper (grade 1) was used to prepare paper discs with a diameter in the range of 6–7 mm. These discs were treated with 20 μL of a Ga-BACD solution (50 mg/mL in PBS, pH 7.4) and incubated overnight in a sealed 96-well plate at room temperature. Following incubation, the discs were washed three times with 10 μL of deionized water and air-dried before being used for further analysis or assays.

2.4. Characterization of Ga-BACDs and Coated Cellulose Paper Discs. The structural characterization of gallium-functionalized boronic acid carbon dots (Ga-BACDs) and modified cellulose-based substrates was conducted to confirm the successful synthesis of carbon dots and the attachment of gallium onto the carbon dots. Optical properties were analyzed using UV–visible spectroscopy (Shimadzu UV-1800) to record absorption spectra of Ga-BACD, while fluorescence emission characteristics were analyzed using a fluorescence spectrometer (FLSP920, Edinburgh Instruments). The surface charge of synthesized carbon dots and colloidal stability were assessed via zeta potential measurements using an Anton Paar Litesizer 500 with a minimum of 60 scans.

Functional group identification in Ga-BACDs was performed using a PerkinElmer FTIR spectrometer using Fourier transform infrared (FTIR) spectroscopy. For FTIR analysis, carbon dots were homogenized with potassium bromide (KBr) in a 1:100 mass ratio, finely ground using an agate mortar, and compressed into pellets under high pressure for 2–3 min. Spectral data were recorded with the pure KBr pellet as the background reference.

High-resolution transmission electron microscopy (HR-TEM) analysis was performed by using a JEOL JEM-2100 microscope equipped with a GATAN ORIUS SC600A camera. The instrument operated at an accelerating voltage of 200 kV, with a camera length of 499.606 mm and a resolution of 0.24 nm. For sample preparation, a drop of a Ga-BACD dispersed solution was deposited onto a carbon-coated copper grid (200 mesh) and left to dry at room temperature until the solvent had completely evaporated. The prepared grid was then mounted on the TEM holder for imaging. Structural analysis on Ga-BACDs was further examined using ultrahigh-resolution scanning electron microscopy (UHR-SEM, TESCAN Magna GMU) (energy of 7 keV, magnifications of 17.9 and 28.3 kx, and working distances of 6.04 and 5.43 mm) coupled with an Oxford AztecLive energy-dispersive X-ray spectroscopy (EDX) system equipped with an Ultimex 65 mm² SSD-ED detector. For SEM analysis, a droplet of the Ga-BACD dispersion was deposited onto a silica wafer and allowed to dry under ambient conditions before imaging. The SEM analysis was performed at an accelerating voltage of 10 kV. Additionally, EDX elemental mapping confirmed the successful incorporation of gallium within the Ga-BACDs.

Inductively coupled plasma–atomic emission spectroscopy (ICP-AES) was employed to quantify gallium in Ga-BACDs. A Shimadzu ICPE-9820 plasma atomic Emission spectrometer was used under the following parameters: a radio frequency power of 1.20 kW, a plasma gas flow of 10.0 L/min, an auxiliary gas flow of 0.60 L/min, and a carrier gas flow of 0.70 L/min. The spectrometer was equipped with axial and radial viewing capabilities and a mini torch. The gadget provides a broad

measurement wavelength range of 167–800 nm, integrating an Echelle spectrometer with a semiconductor CCD detector. A 27 MHz high-frequency source operating at a maximum output of 1.6 kW powered the device. Axial view mode with broad sensitivity was configured for an exposure duration of 30 s. The rinsing technique employed a peristaltic pump operating at 20–60 rpm, comprising a 30 s solvent rinse followed by a 50 s sample rinse.

Both BACD and Ga-BACD samples were analyzed along with a standard gallium calibration. Each sample contained 1 mg of CDs dissolved in 1 mL of ultrapure water, subsequently diluted with 49 mL of 1 M nitric acid (HNO_3), resulting in a final volume of 50 mL. To ensure complete digestion and removal of excess acid, the solutions were heated on a hot plate for 2 h at 60 °C. The solutions were initially filtered using Whatman no. 1 filter paper and subsequently passed through a 0.22 μm syringe filter twice to remove particle debris after cooling. Standard gallium concentrations of 0, 0.1, 0.5, 1, 2.5, and 5 ppm established a calibration curve for ICP readings.

Raman spectroscopy was conducted using a WITec confocal Raman microscope- α 300. The measurements were carried out with a laser power of 65 mW at a wavelength (λ) of 785 nm. A 10 \times magnification objective was used with an integration time of 10 s and an accumulation time of 10 s per spectrum.

Powder X-ray diffraction (XRD) analysis was performed using a Panalytical X'Pert3 Pro multipurpose diffractometer equipped with Cu K α radiation. Data were collected over a 2θ range of 5–50° to determine the crystallographic characteristics of the samples. Lyophilized powder samples were used for the analysis.

X-ray photoelectron spectroscopy (XPS) analysis of the Ga-BACD sample was recorded using an ESCALAB 250 spectrometer with a monochromatic X-ray source with Al K α excitation. Binding energy calibration was based on C 1s at 284.9 eV.

The surface morphology of Ga-BACD-modified paper discs was analyzed by using a VEGA3 scanning electron microscope (SEM, TESCAN). Before imaging, the cellulose-based paper samples were sputter-coated with a thin gold layer to enhance the electrical conductivity. The elemental composition of the modified paper discs was characterized via energy-dispersive X-ray spectroscopy (EDS, Oxford). Quantification of the Ga-BACD coating was performed by using absorption spectroscopic analysis. A Ga-BACD stock solution (50 mg/mL) was prepared, and paper discs were incubated overnight in this solution. Following incubation, the absorbance of the treated solution was measured, and the Ga-BACD quantity on the paper discs was calculated by comparing the absorbance values of the original and treated solutions. The observed decrease in absorbance in the wells containing the paper discs confirmed the attachment of Ga-BACD to the paper. The absorbance difference between the treated and control solutions was used to estimate the amount of carbon dots (CDs) loaded onto each paper disc.

2.5. Antibacterial Properties of Ga-BACDs. The antibacterial properties of Ga-BACD original solution and Ga-BACD-coated paper discs were performed in a similar way to that described in our previous study.¹⁷

2.5.1. Bacterial Inhibition Assays with Ga-BACD Solution. The inhibitory concentrations (IC) of Ga-BACD, which is the measure of potency of a substance inhibiting bacterial growth,⁴⁴ specifically IC₅₀ and IC₉₀, were checked for bacterial cells SE and *E. coli* in a 96-well plate. An overnight seed culture was prepared for each bacterial strain, and 1% was inoculated into a new

presterilized Mueller Hinton broth (MHB) tube. The optical density (OD) was monitored at A_{600} until it reached 0.22 (1×10^8 CFU/mL). Ga-BACDs were diluted in PBS (pH 7.4) from a 50 mg/mL stock to get a range of concentrations (final concentrations of 25, 10, 5, 4, 2.5, 1, and 0.1 mg/mL). Each well contained 50 μ L of bacterial suspension (1×10^6 CFU/mL), resulting in a bacterial final concentration of 1×10^5 CFU/mL. The blank (PBS/MHB) and cell culture control were included in the bacterial assay. Gentamicin-treated culture wells were included as a positive control for the assay. After a 120 min incubation at room temperature, plates were incubated overnight at 37 °C. Bactericidal activity was assessed by comparing the A_{600} readings of treated and control wells using a BioTek 800TS microplate reader, using eq 1.^{45,46} Background corrections were done using the mean absorbance value of the PBS/MHB media blanks. The decrease in absorbance indicated the bactericidal effect of the CDs. IC_{50} and IC_{90} values were determined by plotting the percentage growth of cells against CD concentration for each bacterial strain. The IC values were calculated using GraphPad Prism's (version 8.4.3) nonlinear regression curve fit through dose–response inhibition analysis. Culture viability was calculated using the following relationship:

$$\% \text{ culture viability} = \left(\frac{\text{mean absorbance of treated wells}}{\text{mean absorbance of control wells}} \times 100 \right) \% \quad (1)$$

2.5.2. Bacterial Inhibition Assays with Ga-BACD Paper Discs. To evaluate the bioactivity of CD-modified paper discs and their ability to inhibit bacterial growth, an agar plate assay was conducted. The initial assay was conducted with varying concentrations of Ga-BACD for paper disc coating (50, 20, 10, and 5 mg/mL). The modified discs were exposed to a bacterial suspension (20 μ L; 5×10^5 CFU/mL) and incubated for 2 h at room temperature under dark conditions. After incubation, the solution in the well underwent serial dilution (5 \times with PBS, followed by 50 \times), and 10 μ L of the final dilution was plated onto MHB agar for overnight incubation at 37 °C. To further assess growth inhibition, the paper disc from the well was also transferred to the agar plate. Control experiments with unmodified discs were performed for comparison. Bacterial growth on the plates was examined to determine the antimicrobial effectiveness of CD-modified discs.

2.5.3. SEM Imaging on Bacterial Cells to Study the Cell Morphological Changes. The surface morphological changes of bacteria (*E. coli* and SE) induced by Ga-BACD treatment were analyzed using high-resolution scanning electron microscopy (SEM). A 10 mg/mL solution of GACD was used for the bacterial treatment. Both the treated and control bacterial cultures (10^5 cells/mL) were incubated at 37 °C for 3 h. Following the incubation period, the cells were harvested and washed with sterile phosphate-buffered saline (PBS, pH 7.4). Both control and Ga-BACD-treated bacterial cells were fixed with a 2.5% glutaraldehyde solution at 4 °C for 4 h. The fixed samples were then washed and subjected to a graded ethanol dehydration series (25, 30, 50, 70, 80, 90, and 100%) before drying. The dried samples were mounted onto SEM stubs by using double-sided carbon tape. To enhance conductivity, a thin layer of gold (5–10 nm thickness) was sputter-coated onto the samples before imaging using SEM.

2.6. Bacterial Biofilm Assays. **2.6.1. Biofilm Inhibition Assay.** To evaluate biofilm formation in the presence of Ga-

BACD, the Gram-positive SE and Gram-negative *E. coli* cultures were treated with carbon dot solution at concentrations ranging from 0.1 to 25 mg/mL, similar to the protocol described in Section 2.5.1. After 48 h of incubation, total biomass, planktonic growth, and biofilm formation were quantified using spectrophotometric analysis with a BioTek 800TS microplate reader.

Total microbial growth was determined by measuring each well's optical density at 600 nm following the incubation period. Planktonic phase growth was quantified by transferring the liquid culture medium to a separate 96-well plate and measuring its absorbance. Biofilm formation was evaluated using crystal violet staining, following previously reported methodologies.²¹ Briefly, the adherent biofilm in the original microplate was washed with deionized water and subsequently stained with 100 μ L of a 0.1% crystal violet solution for 20 min. The excess stain was removed, and the wells were washed twice with 200 μ L of deionized water. The stained biofilms were then eluted using 200 μ L of absolute ethanol with agitation at 120 rpm for 10 min. The eluted crystal violet solution was transferred to a new 96-well plate, and the absorbance was measured at 575 nm to quantify biofilm formation.

2.6.2. Biofilm Eradication Assay. To assess the effectiveness of Ga-BACDs in eradicating bacterial biofilms, untreated broth cultures of *Staphylococcus epidermidis* (SE) and *E. coli* were incubated in a 96-well plate for 72 h, allowing for thick biofilm formation. After incubation, the planktonic growth was removed and replaced with fresh media (MHB). The cultures were then treated with Ga-BACDs at varying concentrations (0–25 mg/mL). Plates were incubated for another 72 h, and total growth, planktonic growth, and biofilm formation were then quantified via a crystal violet staining method as described in Section 2.6.1.

2.7. Cytotoxicity Studies on Human Cell Lines. To evaluate the cytotoxic effects of Ga-BACD solutions and Ga-BACD-modified paper discs, we used human brain microvascular endothelial cell (HBMEC) lines. Cellular metabolic activity was quantified using the MTT assay, as described in our previous studies.^{17,18} Experimental conditions included 96-well plates for the solution-based assay and 24-well plates for a paper disc assay. HBMEC cells were seeded at cell densities of 10,000 per well (96-well plates) and 50,000 cells per well (24-well plates) in DMEM complete medium and incubated overnight under controlled conditions (37 °C, 5% CO₂, and $\geq 95\%$ relative humidity).

Following incubation, the medium was replaced with fresh medium containing Ga-BACD at concentrations of 0.1, 0.5, 1.0, 5.0, and 10.0 mg/mL in triplicates. Untreated cells were considered as the control, while cells treated with 10% DMSO served as the positive inhibition control. In parallel, modified and unmodified control paper discs were added to the 24-well plates. After 48 h of exposure, an MTT solution (5 mg/mL in PBS) was added, with a final concentration of 0.5 mg/mL, and the plates were incubated for an additional 4 h. Subsequently, 200 μ L (96-well plates) or 500 μ L (24-well plates) of DMSO was added to solubilize the formazan product, and the plates were maintained in darkness at room temperature for 10–15 min. Absorbance readings were recorded at 570 nm by using a BioTek 800TS microplate reader. Each experiment was performed in triplicate by using three independent batches of Ga-BACDs. Cell viability was determined by comparing the absorbance values of Ga-BACD-treated wells to those of untreated control wells, using eq 1. To minimize contamination, Ga-BACD coating to the paper discs was done in a laminar flow hood sterile condition. Unmodified control discs underwent the

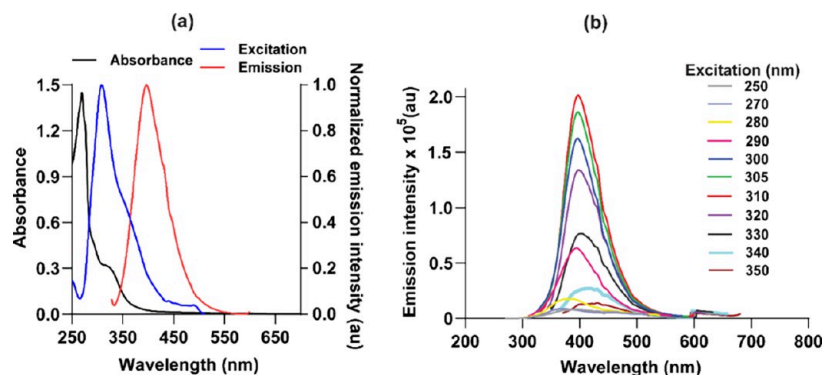


Figure 1. Absorbance and emission profiles of Ga-BACDs. (a) UV-vis absorbance spectra showing absorption peaks at (left Y axis, black spectra). Excitation (blue) and emission spectra (red) of Ga-BACDs (right Y-axis, ex-310 nm; the em range is 330–600 nm). (b) Emission of Ga-BACDs at different excitation wavelengths, from 250 to 350 nm.

same procedural steps to ensure consistency under experimental conditions.

2.8. Statistical Analysis. All bacterial assays and cytotoxicity tests were performed using three distinct batches of freshly prepared CDs, with each experiment conducted in triplicate. Statistical analysis was carried out using GraphPad Prism (ver. 8.4.3), and data comparisons between different treatment conditions were analyzed using the ANOVA test.

3. RESULTS AND DISCUSSION

3.1. Synthesis and Characterization of Ga-BACDs.

Carbon-based nanomaterials, particularly metal-doped carbon nanoparticles, have gained significant attention considering their exceptional fluorescence properties and diverse applications in medical and related industries.^{20,37,47} These materials exhibit remarkable electrochemical, photothermal, antibacterial, antifungal, bioimaging, and antitumor applications.⁴⁸ Our previous research on phenylboronic acid carbon dots (BACDs) demonstrated significant antibacterial properties.¹⁷ The incorporation of boronic acid contributed to strong bacterial binding affinity and potentially enhanced ROS-mediated bacterial destruction.⁴⁹ By doping BACD carbon dots with gallium (Ga), a metal with known antibacterial and biofilm resistance properties,⁵⁰ we aimed to enhance their efficacy for combating bacterial infections, particularly in the context of biofilm-related antimicrobial resistance.

The optimal synthesis conditions for Ga-BACDs were sonication at 20 kHz and 2000 W for 60 min at a 60% amplitude and 60 °C, yielding the highest gallium incorporation or dispersal on BACDs (the experimental setup is shown in Figure S1). The precipitates were separated postsonication, and detailed optical and structural characterizations were conducted before evaluating their functional applications. UV-vis spectroscopy confirmed distinct absorbance peaks at 286 and 355 nm (Figure 1a), consistent with BACDs.¹⁷ Fluorescence emission spectra recorded at different excitation wavelengths of 250–350 nm (Figure 1b) revealed that Ga-BACDs exhibited maximum fluorescence when excited at 308 nm, with a prominent emission peak at 397–400 nm, characteristic of carbon dots (Figure 1a).

The successful doping of gallium onto BACDs was confirmed through FTIR spectroscopy, which showed variations in the spectral patterns, indicating modifications in surface functional groups. Figure 2 illustrates the functional groups present in the synthesized Ga-BACDs (pink spectra) in comparison with undoped BACDs (green-colored spectra). Both samples

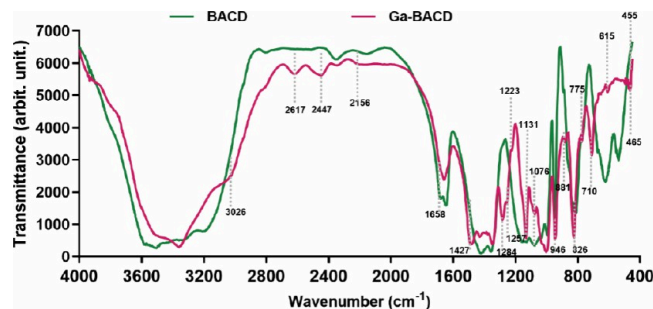


Figure 2. FTIR spectra of Ga-BACDs (pink) compared with BACD spectra (green). The signals indicated with dashed lines represent the new shifts in characteristic peaks that show gallium doping on BACDs.

exhibited characteristic common peaks at specific wavenumbers (3200 cm^{-1} for O–H and 1340 , 1190 , and 1020 cm^{-1} for B–O), confirming the presence of fundamental functional groups. However, the introduction of gallium resulted in notable peak shifts and the formation of new peaks marked with dotted lines, further supporting the surface modification caused by gallium doping. The additional peaks (Figure 2) in the 2000 – 2600 cm^{-1} range indicate the formation of Ga–H or Ga–O–C interactions, potentially resulting from interactions between gallium and organic functional groups within the carbon dot framework.⁵¹ The new bands visible in the 400 – 700 cm^{-1} range suggest Ga–O and Ga–O–Ga lattice vibrations, which are typical of gallium oxide phases.⁵² Specifically, the peak at 455 cm^{-1} suggests the presence of the Ga–O group.⁵³ Additionally, peaks at the 1400 – 1600 cm^{-1} range are indicative of C=C stretching vibrations in graphitic domains and possible interactions between gallium and aromatic structures, hence affirming the incorporation of gallium into the carbon dot network.⁵⁴

Zeta potential analysis provides a quantitative measure of the surface charge of nanoparticles, which plays a significant role in predicting their aggregation behavior, colloidal stability, dispersion, and interactions in solutions.⁵⁵ The zeta potential value of gallium-doped carbon dots (Ga-BACDs) was found to be $-23.3 \pm 1.53\text{ mV}$, in contrast to the more negative value of $-32.5 \pm 1.69\text{ mV}$ observed for undoped BACDs. The less negative zeta potential of Ga-BACDs relative to BACDs indicates that gallium doping modulates the surface charge, likely through modifications in the functional group (carboxyl or hydroxyl) composition or electrostatic interactions.

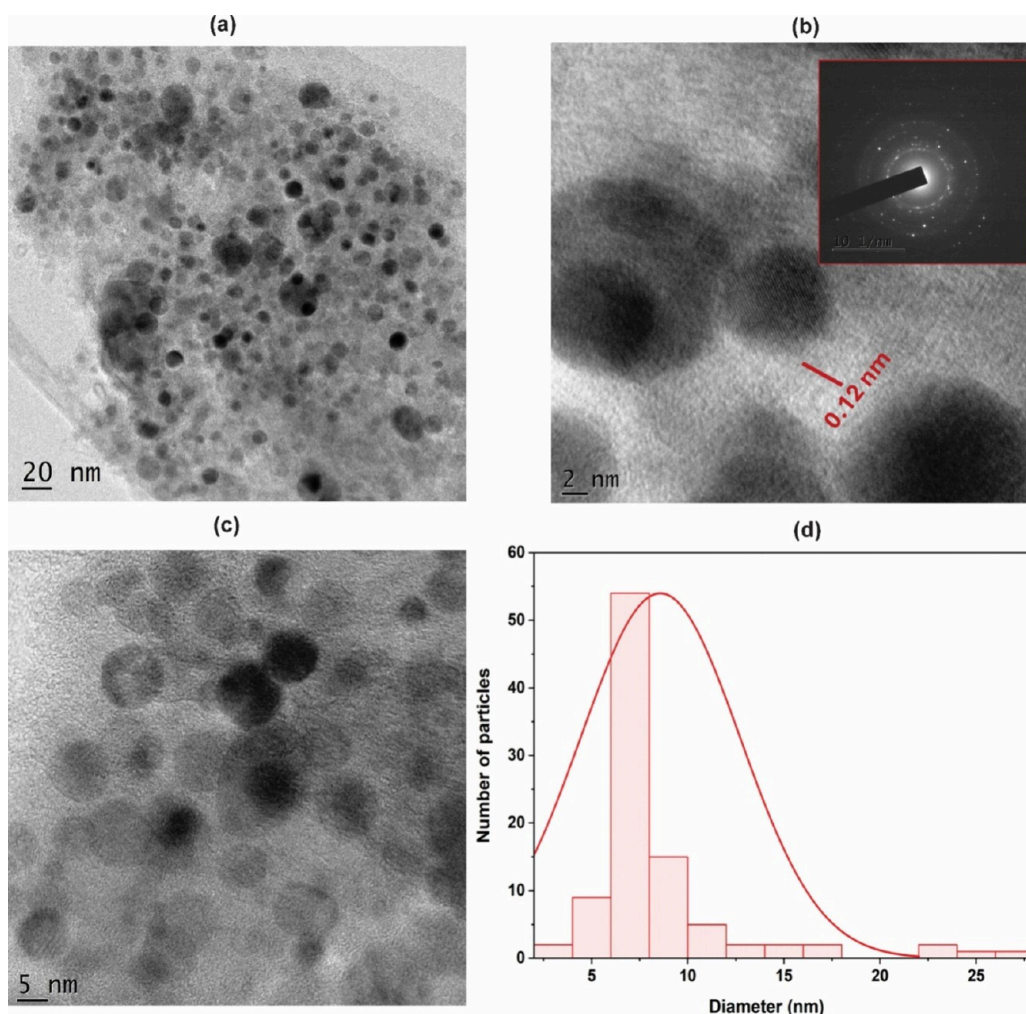


Figure 3. HR-TEM images of Ga-BACDs. (a) TEM micrograph of the Ga-BACDs. (b, c) HR-TEM images confirming the crystalline pattern for the carbon dots with an interplanar spacing of 0.12 nm. Inset: SAED pattern of Ga-BACDs. (d) Histogram showing particle size distribution for (c); here Ga-BACDs revealing the size range of 2–26 nm with an averaged diameter of Ga-BACDs of 8.57 ± 4.1 nm.

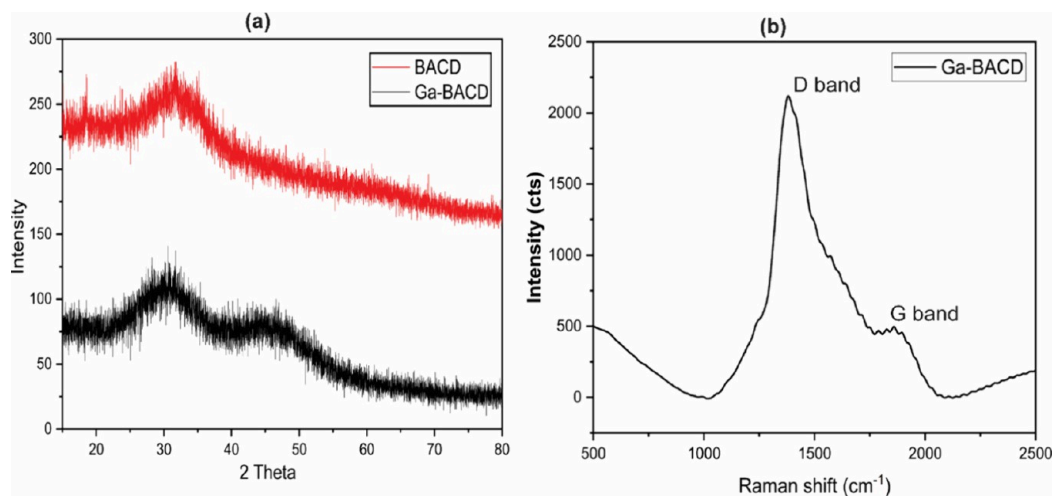


Figure 4. XRD and Raman spectroscopy analysis on Ga-BACDs. (a) XRD spectra of doped (Ga-BACD) and undoped (BACD) and (b) Raman spectral analysis on Ga-BACDs showing the D- and G-band of carbon material.

The sonochemical method efficiently synthesizes well-defined, polycrystalline Ga-carbon dots with controlled size distribution.^{43,56} The synthesis of fluorescent Ga-BACDs was

successfully achieved by sonicating molten gallium in a BACD solution.

High-resolution TEM (HR-TEM) images (Figure 3a,c) clearly show the formation of well-defined nanostructures,

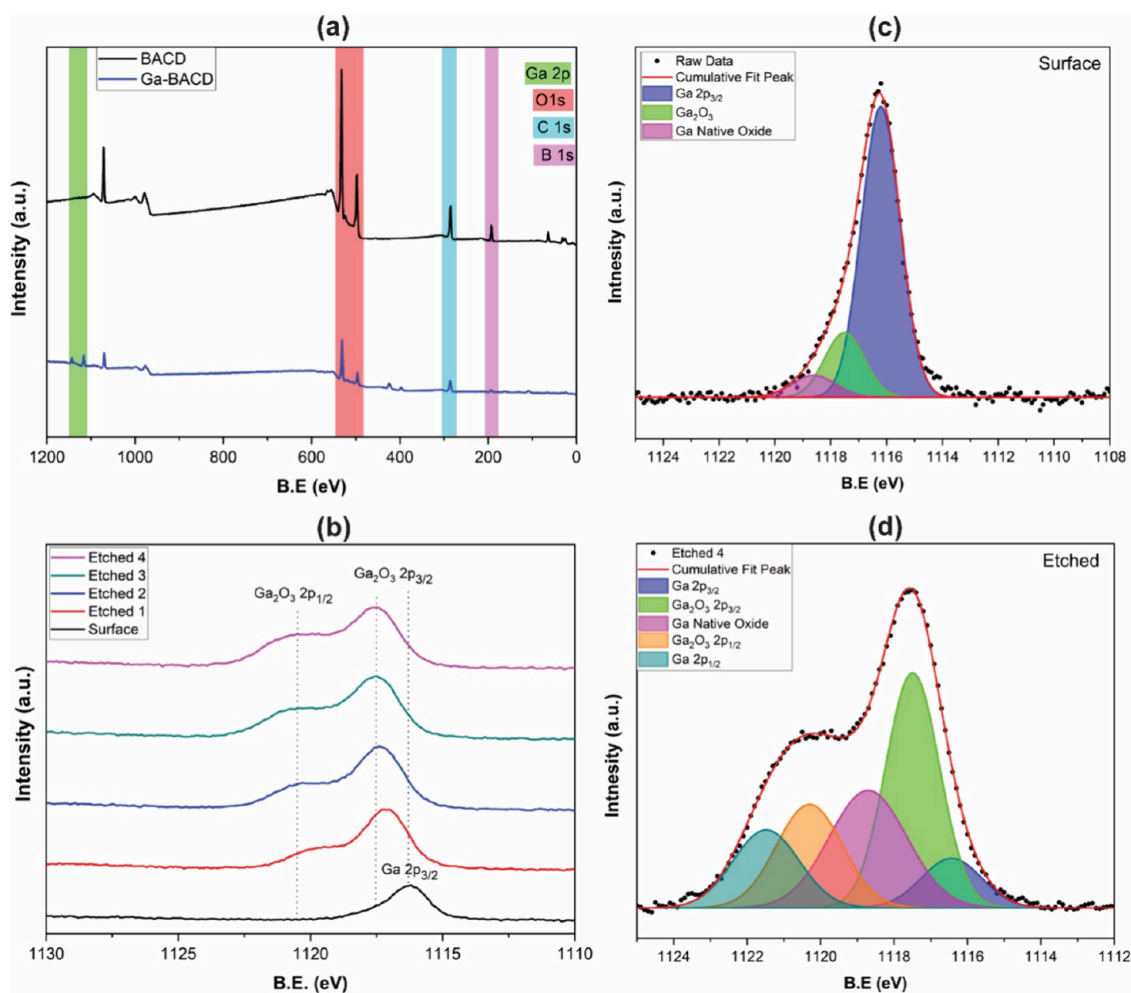


Figure 5. XPS analysis on Ga-BACDs. (a) Survey XPS spectra of BACDs and Ga-BACDs, demonstrating the constituent composition prior to and after to gallium incorporation. (b) The XPS depth profile compares the Ga 2p signal from the as-synthesized surface to the fourth etched layer, illustrating the retention of Ga beneath the outermost carbon shell. (c) High-resolution Ga 2p spectrum of the synthesized Ga-BACD surface deconvoluted into constituents. (d) High-resolution Ga 2p spectrum after four cycles of Ar⁺ etching, demonstrating the heightened intensity of subsurface Ga₂O₃ species and validating the presence of lattice-embedded Ga.

where gallium nanoparticles are embedded within or coated by a carbonaceous shell, confirming the hybrid nature of Ga-BACDs. The HR-TEM lattice fringes having interplanar spacings of 0.243, 0.207, and 0.123 nm correspond to the (100), (101), and (110) planes of hexagonal graphitic carbon (PDF 26-1023), respectively. The Miller indices and *d*-spacing values are consistent with previous reports.^{57,58}

Statistical analysis of the particle size (Figure 3c) shows that the average diameter of the Ga-BACDs is approximately 8.57 ± 4.1 nm. This dimension aligns well with the typical size range of gallium carbon dots reported in an earlier study,⁴³ suggesting consistency and control in the synthesis method. The particle size distribution histogram (Figure 3d), based on measurements from Figure 3c, demonstrates a relatively small count above 12 nm and a narrow distribution between 2 and 26 nm. The 7–8 nm size range has the largest particle counts, suggesting a preponderance of uniformly smaller particles.

The HR-SEM image of Ga-BACD (Figure S2a) provides further confirmation of the hybrid structure observed in the TEM images with Ga-BACD particles showing a slightly larger size compared to the BACD particles.¹⁷ This increase in size is likely due to the incorporation of gallium (Ga), which modifies the particle morphology, supporting the gallium doping.^{59–61}

Additional confirmation of gallium presence was provided qualitatively by EDX (Figure S2b) and quantitatively by ICP-AES. The BACD exhibited no gallium content, while the gallium concentration in the Ga-BACD was determined from the ICP results as 18.3% (w/w).

Figure 4a displays the X-ray diffraction (XRD) patterns of bare amorphous carbon dots (BACDs) and gallium-doped carbon dots (Ga-BACDs). The BACD pattern displays a wide diffraction peak centered at $2\theta = 24.5^\circ$, corresponding to the (002) plane of disordered carbon.⁶² This peak indicates an amorphous carbon configuration characterized by low graphitization and inadequately arranged graphene layers. The absence of pronounced peaks signifies the absence of notable crystalline phases aligned with the amorphous characteristics of the carbon dots. The Ga-BACD sample has a comparable broad peak at around $2\theta = 24.5^\circ$, suggesting that the incorporation of gallium does not substantially modify the fundamental amorphous carbon structure. Nevertheless, a significant secondary peak is observed at around $2\theta = 44^\circ$, potentially corresponding to the (100) plane of carbon, commonly linked to in-plane structural ordering.⁶³ The peak appears in the Ga-BACD sample, indicating that gallium incorporation may improve local

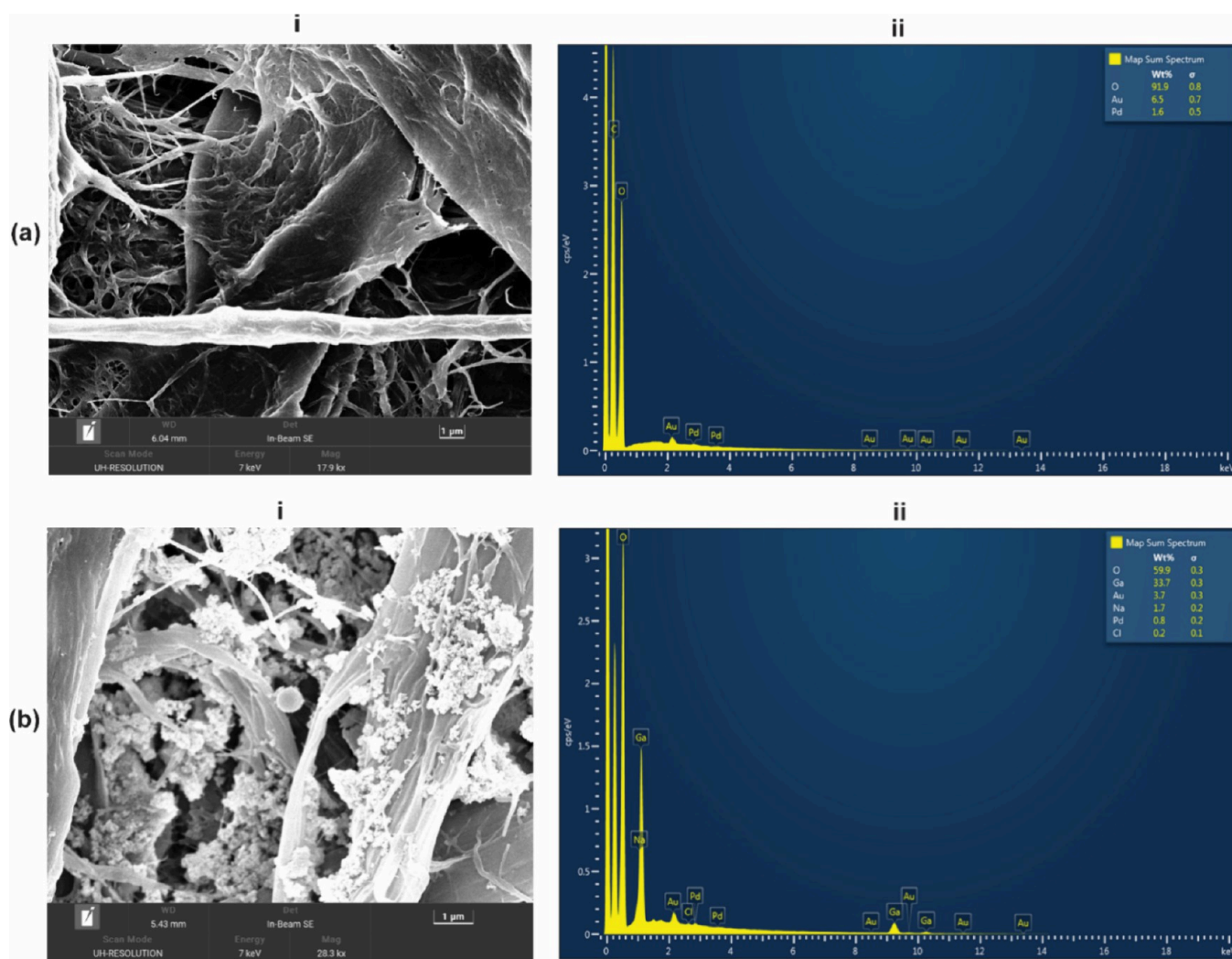


Figure 6. SEM/EDX analysis on a Ga-BACD-coated paper disc. (a) Untreated paper disc (control) and (b) Ga-BACD-coated paper disc: (i) SEM image of a paper disc and (ii) EDX spectrum of a paper disc. The elemental mapping shows the presence of 33.7% gallium in the Ga-BACD-treated disc.

ordering within the amorphous matrix or contribute to scattering effects from gallium–carbon interactions.

The variations in intensity and the emergence of the secondary peak corroborate the idea that gallium is assimilated into the carbon matrix in the form of discrete crystalline gallium or gallium oxide phases. This behavior is characteristic of metal-doped carbon materials, in which metal atoms are either intercalated within the carbon matrix or constitute amorphous complexes.⁴³

Figure 4b displays the Raman spectrum of gallium-doped amorphous carbon dots (Ga-BACD). The spectra display two significant peaks located at roughly 1350 and 1580 cm^{-1} , which correspond to the D-band and G-band, respectively. These bands are indicative of carbon-based materials and offer insights into the structural characteristics and level of disorder within the carbon matrix.¹⁷ The D-band (about 1350 cm^{-1}) originates from disordered carbon and vibrations caused by defects in the sp^2 hybridized carbon network. Its presence signifies structural flaws, including vacancies, grain boundaries, and distortions resulting from doping with heteroatoms, namely gallium. The strength of this band indicates considerable disturbance of the organized graphitic structure. The G-band ($\sim 1580 \text{ cm}^{-1}$) corresponds to the E_{2g} vibrational mode of sp^2 carbon atoms

in graphitic structures, signifying in-plane stretching of carbon–carbon bonds.⁶⁴

The intensity ratio of the D-band to the G-band, denoted as I_D/I_G , offers essential insights into the extent of graphitization (Figure 4b) (the deconvoluted Raman spectra are provided in the supplementary data, Figure S3). The D-band intensity surpasses the G-band intensity, indicating a mostly amorphous carbon structure characterized by a high defect density. This aligns with the structural disturbance identified in the XRD analysis (Figure 4a).

The XPS survey spectra (Figure 5a) of BACD revealed the presence of C 1s at 284.9 eV, O 1s at 532.3 eV,⁴³ and B 1s at 192.23 eV.⁶⁵ The B 1s binding energy is consistent with boronic acid or borate-type species, likely as $\text{B}(\text{OH})_2$ or B_2O_3 -like groups on the carbon dot surface.⁶⁷ Following Ga incorporation, two new peaks appeared in the Ga-BACD survey spectra at 1143.2 and 1116.4 eV, which correspond to Ga 2p_{1/2} and Ga 2p_{3/2}, respectively.⁶⁶ These binding energies indicate that gallium is initially present in a partially oxidized state, potentially interacting with the surface functional groups. After doping with Ga, the peak of B 1s at the surface of Ga-BACD shifted to $\sim 194.0 \text{ eV}$, a +1.7 eV increase compared to BACDs. This shift suggests an electron-deficient boron environment, probably

caused by coordination with Ga³⁺ ions or partially oxidized gallium to form Ga–O–B bonds. Depth profiling by successive Ar⁺ etching (Figure 5b) reveals that the Ga 2p_{3/2} peak intensity increased and progressively shifted from 1116.4 to 1117.7 eV (Figure 5c,d), which is characteristic of Ga³⁺ in Ga₂O₃.⁶⁸ Simultaneously, the B 1s peak shifted further to ~197.0 eV, consistent with a more oxidized and electronically depleted environment. These results indicate that gallium is not simply adsorbed on the surface; instead, the increase in the intensity of the Ga signal during etching implies that the element is embedded within the carbon dot matrix, probably via Ga–O–B or Ga–O–C networks, rather than being confined to surface-bound species only.

3.2. Characterization of Ga-BACD-Modified Cellulose.

The presence of polysaccharides, primarily cellulose, in the extracellular polymeric substances (EPS) of biofilms makes cellulose an important target for antimicrobial strategies.^{14,69} Since our previous study has shown that BACDs retain their bioactivity when attached to cellulose surfaces,¹⁷ this study further confirms the activity of Ga-BACDs on cellulose substrates. To check this, cellulose paper was coated with Ga-BACD solutions (50 mg/mL), following the protocol outlined in Section 2.3. The amount of CDs deposited on the cellulose was found to be 255.7 ± 47.8 μg per milligram of cellulose, as measured by UV spectrophotometric analysis. The successful deposition of Ga-BACDs on the cellulose substrate was further verified by using HR-SEM and EDX. SEM imaging showed the presence of nanoparticles on the cellulose surface (Figure 6b(i)), in contrast to the untreated cellulose (Figure 6a(i)), and EDX analysis (Figure 6b(ii)) confirmed the presence of gallium (Figure 6a(ii)). This effective surface modification suggests that Ga-BACD-functionalized cellulose could be a novel alternative for antimicrobial application materials for preventing biofilm formation and microbial contamination.

3.3. Antibacterial Studies. The antibacterial efficacy of Ga-BACD was tested against two model bacterial species: the Gram-negative bacterium *Escherichia coli* (*E. coli*) and the Gram-positive bacterium *Staphylococcus epidermidis* (SE). The experiment involved treating these bacterial cultures with varying concentrations of Ga-BACD solution (0–25 mg/mL), as described in Section 2.5.1. The initial 2 h incubation at room temperature allowed better interaction between the bacterial membrane and carbon dots thereby promoting their potential binding prior to the enhancement of metabolic activity at 37 °C.^{17,70} Gentamicin-treated culture wells (GM) were considered as a positive inhibition control for the assay. A dose-dependent decrease in bacterial growth was observed with increasing concentrations of Ga-BACD. Ga-doped BACDs exhibited superior antibacterial activity compared to undoped BACDs against both SE (Figure 7a) and *E. coli* (Figure 7b). The inhibitory concentrations (IC₅₀ and IC₉₀) are summarized in Table 1. The IC₉₀ value for Ga-BACD against SE was found to be 3.2 ± 0.28 mg/mL, which is approximately half of the IC₉₀ value observed for BACD (6.52 ± 0.58 mg/mL), indicating enhanced antibacterial activity of Ga-BACD. Similarly, for *E. coli*, the IC₉₀ value for Ga-BACD treatment was 2.22 ± 0.10 mg/mL, significantly lower than that of BACD (4.72 ± 0.17 mg/mL), further confirming the superior antibacterial efficacy of Ga-BACDs. The enhanced antibacterial activity can be attributed to gallium's ability to disrupt bacterial iron metabolism, a mechanism previously reported in *Pseudomonas aeruginosa*.³⁹ Additionally, the increased antibacterial effect of carbon nanoparticles,⁷¹ especially metal-doped variants like Ga-

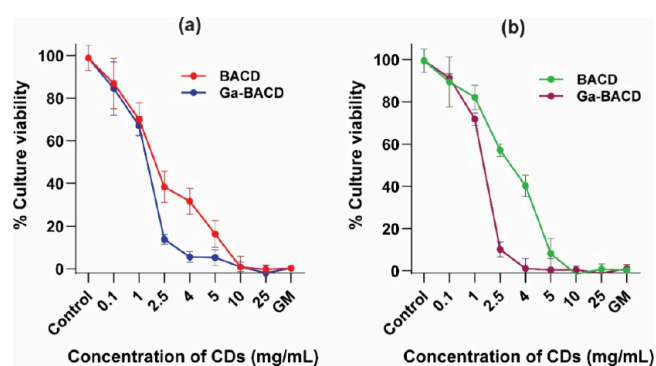


Figure 7. Antibacterial assay with BACDs and Ga-BACDs against (a) *Staphylococcus epidermidis* (SE) and (b) *Escherichia coli*. Control represents the untreated culture wells, and GM represents the culture well treated with antibiotic gentamicin (positive control). Each point represents the mean ± SD, calculated from three different experiments.

Table 1. Minimum Inhibitory Concentrations (IC₉₀ and IC₅₀) of Ga-BACDs and BACDs against Bacteria

type of CD	IC ₉₀ (mg/mL)		IC ₅₀ (mg/mL)	
	SE	<i>E. coli</i>	SE	<i>E. coli</i>
BACD	6.52 ± 0.58	4.72 ± 0.17	1.87 ± 0.28	3.05 ± 0.26
Ga-BACD	3.2 ± 0.28	2.22 ± 0.10	1.25 ± 0.11	1.35 ± 0.14

BACDs, is primarily driven by the generation of reactive oxygen species (ROS), such as hydroxyl radicals and singlet oxygen. These ROS cause oxidative stress, damaging key bacterial components like DNA, RNA, proteins, and lipids, leading to mitochondrial dysfunction, protein deactivation, and lipid peroxidation, ultimately resulting in bacterial cell death through apoptosis or necrosis.^{2,6,12}

HR-SEM images of Ga-BACD-treated bacteria (Figure 8a,b; treated) show significant structural damage, including membrane rupture and surface irregularities, which contrast with the intact surfaces of untreated Gram-negative bacteria *E. coli* (Figure 8a, untreated) and Gram-positive SE (Figure 8b, untreated). This membrane disruption increases bacterial permeability, causing cytoplasmic leakage and accelerating cell death. These results validate Ga-BACDs as a promising antibacterial tool against both Gram-positive and Gram-negative bacteria.

3.4. Antibacterial Studies of Ga-BACD-Modified Cellulose. The antimicrobial activity of Ga-BACD-modified cellulose was evaluated and compared with BACD-modified cellulose, following the protocol outlined in Section 2.5.2. Cellulose discs were coated with solutions of CDs at an optimal concentration of 50 mg/mL (Figure S4) leading to a loading of 255.7 ± 0.0478 μg CDs per mg of cellulose fibers. The modified discs were incubated with bacterial solutions for 2 h, and the growth of bacteria was monitored in solution and on the surface of the fibers.

The results (Figure 9) showed complete bacterial inhibition by Ga-BACD-modified cellulose with no visible bacterial growth around the coated discs or in the treated solution. In contrast, BACDs exhibited reduced antibacterial activity under darker conditions, with bacterial colonies forming around the coated disc and in the treated solution resembling those of the control disc. These findings highlight the enhanced antibacterial potential of Ga-BACD-functionalized cellulose, suggesting it as a promising material for developing advanced antimicrobial

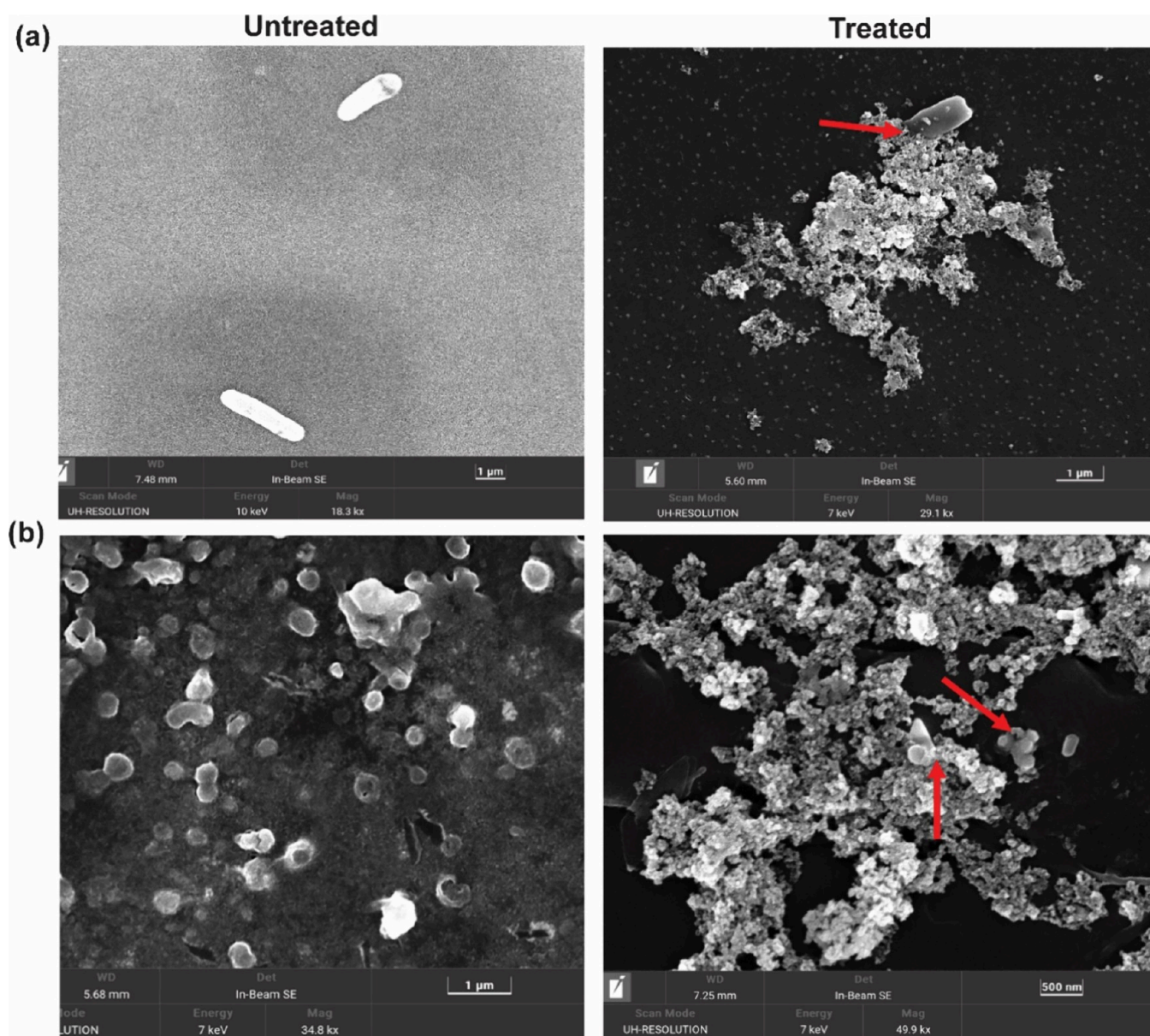


Figure 8. Ultrahigh-resolution SEM images of bacteria: the images compare untreated bacteria with those treated using Ga-BACD. The treatment was done to (a) *Escherichia coli* and (b) *Staphylococcus epidermidis* (SE). Morphological changes or damage induced by Ga-BACD treatment are indicated with arrows.

surfaces or protective coatings, particularly in biomedical and environmental settings.

3.5. Bacterial Biofilm Inhibition Assay. Bacterial biofilms play a major role in antimicrobial resistance by providing a protective environment for bacteria, making them highly resistant to both conventional antibiotics and immune system defenses. These biofilms, formed through exopolysaccharide secretion, enhance bacterial adhesion and greatly increase resistance to antimicrobial agents.^{8,72} The formation of biofilms on medical devices presents a major challenge in healthcare, highlighting the need for advanced antimicrobial strategies.²³

Our study extended to investigate the potential of gallium-doped carbon dots (Ga-BACDs) to inhibit the biofilm for the selected model microbes *Escherichia coli* (*E. coli*) and *Staphylococcus epidermidis* (SE). By treating with varying concentrations of Ga-BACDs in bacterial cultures, as per the procedure outlined in Section 2.6.1, we assessed the potential of Ga-

BACDs on growth and biofilm inhibition. The growth and biofilm formation of *E. coli* and SE were induced at 28–30 °C in MHB broth, with treatment at various Ga-BACD concentrations. Within each well, inoculated with bacterial cultures, total growth comprised both planktonic phase proliferation (bacteria suspended in liquid culture media) and biofilm-associated bacteria (adherent to the bottom and side surfaces of the well).

Bacterial growth in both the total and planktonic phases was assessed by measuring the absorbance at 600 nm. By comparing bacterial growth across these phases following 48 h of incubation, the specific inhibitory effects of Ga-BACD treatment on *E. coli* and *Staphylococcus epidermidis* (SE) proliferation were calculated.

Figure 10 shows the total bacterial growth and planktonic phase growth patterns, with SE data in Figure 10a(i) and *E. coli* data in Figure 10b(i). Ga-BACD treatment resulted in a

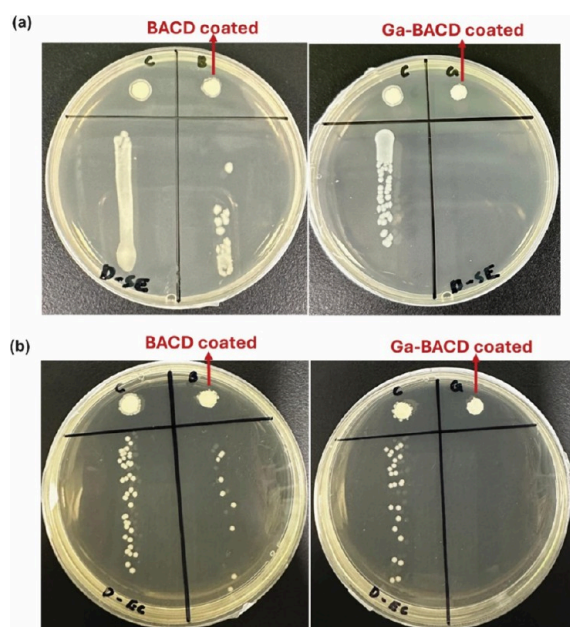


Figure 9. Antibacterial assay with BACD- and Ga-BACD-coated paper discs against (a) *Staphylococcus epidermidis* (SE) and (b) *Escherichia coli*. The Ga-BACD-coated disc has shown a stronger antibacterial effect compared to the BACD paper disc.

statistically significant reduction in total bacterial proliferation at all concentrations ≥ 1 mg/mL ($p < 0.0001$) (Figure 10a(i)). A gradual decrease in planktonic growth was observed at

concentrations ranging from 1 to 25 mg/mL, indicating a direct inhibitory effect of Ga-BACDs on bacterial growth.

The biofilm formed from untreated SE and *E. coli*, quantified via crystal violet staining and measured at 575 nm, was normalized to 100%. Upon treatment with 2.5 mg/mL Ga-BACDs, SE biofilm formation exhibited a progressive decline to 20% within 48 h, with complete inhibition occurring at concentrations ≥ 10 mg/mL for both SE (Figure 10a(ii)) and *E. coli* (Figure 10b(ii)). Furthermore, at Ga-BACD concentrations of 25 and 10 mg/mL, no detectable biofilm formation was observed for either bacterial strain. Figure S5 shows the inhibition of biofilm formation on the coverslip surface at a concentration of 10 mg/mL, comparing biofilm growth in the control sample to that in the Ga-BACD-treated SE strain.

Bright-field microscopy imaging (with a Leica DMI1 bright-field microscope) further confirmed the concentration-dependent inhibition of biofilm formation in both *Staphylococcus epidermidis* (SE) (Figure 11) and *E. coli* (Figure S6). At 2.5 mg/mL of Ga-BACDs, approximately 20% of biofilm growth remained compared to the untreated control, while concentrations of ≥ 10 mg/mL resulted in complete biofilm inhibition (Figures 10a(ii) and 11). At concentrations exceeding 2.5 mg/mL, minimal biofilm formation was observed for both *E. coli* and SE, demonstrating that Ga-BACDs effectively inhibit biofilm formation at concentrations above this threshold. Figure S7 presents a photograph showing the layout of a 96-well plate crystal violet staining assay, demonstrating a gradual reduction in biofilm formation with increasing Ga-BACD concentration.

3.6. Biofilm Eradication Assay. To evaluate the biofilm eradication potential of Ga-BACDs, untreated bacterial cultures

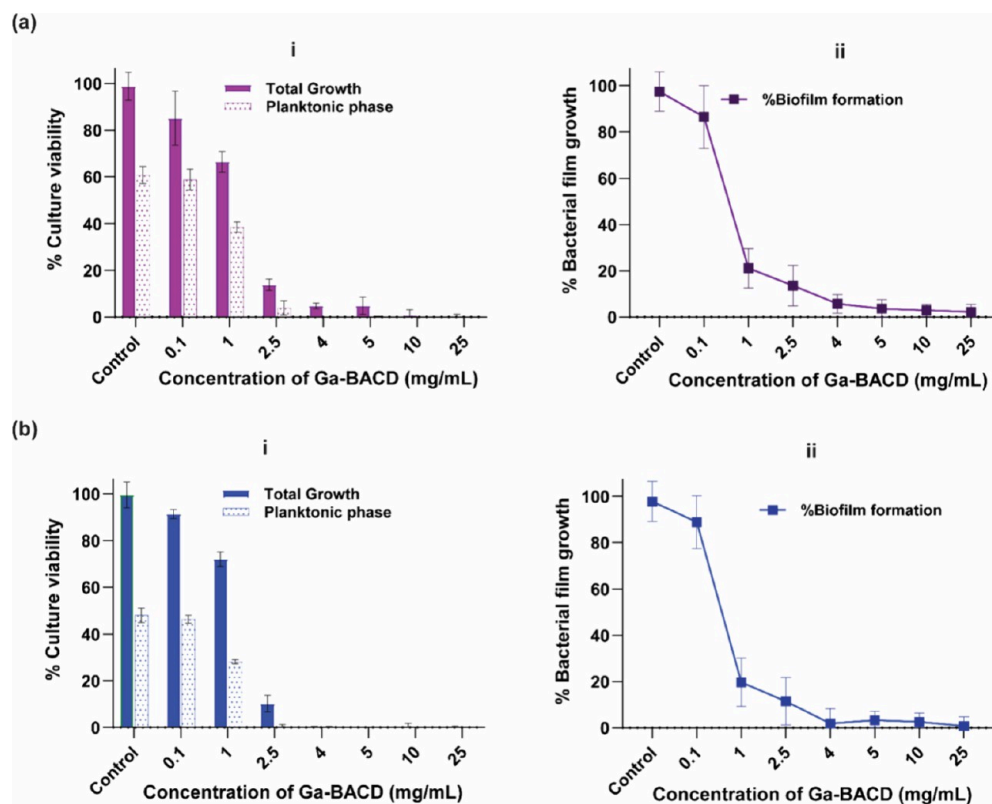


Figure 10. Antibiofilm properties of Ga-BACDs against (a) Gram-positive (SE) and (b) Gram-negative bacteria (*E. coli*). Microbes were treated with Ga-BACDs at varying concentrations of CDs (0.1–25 mg/mL). Cultures were incubated for 48 h, at which time (i) the total planktonic and (ii) biofilm growth was quantified. Experiments were performed in triplicate, and each point represents the statistical averaged value (mean \pm SD).

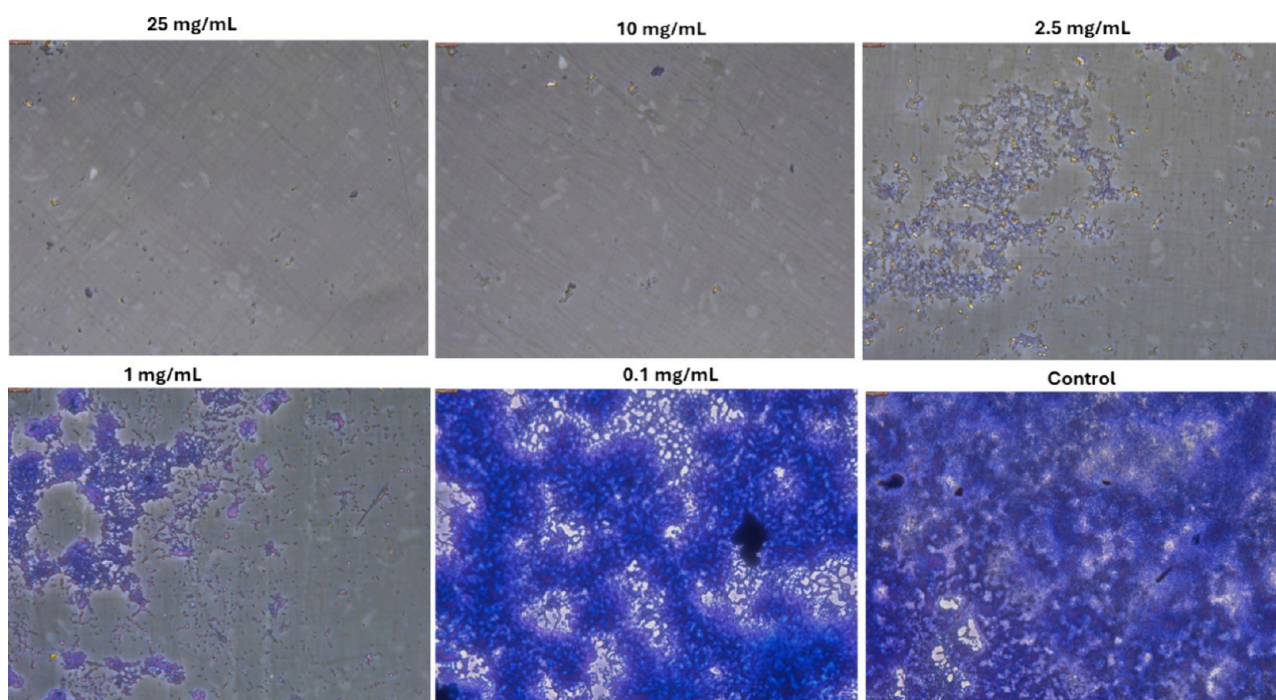


Figure 11. Bright-field microscopy images of crystal violet-stained biofilm (*Staphylococcus epidermidis*). Ga-BACDs effectively inhibited bacterial biofilm formation on well surfaces at concentrations of 1 mg/mL and higher.

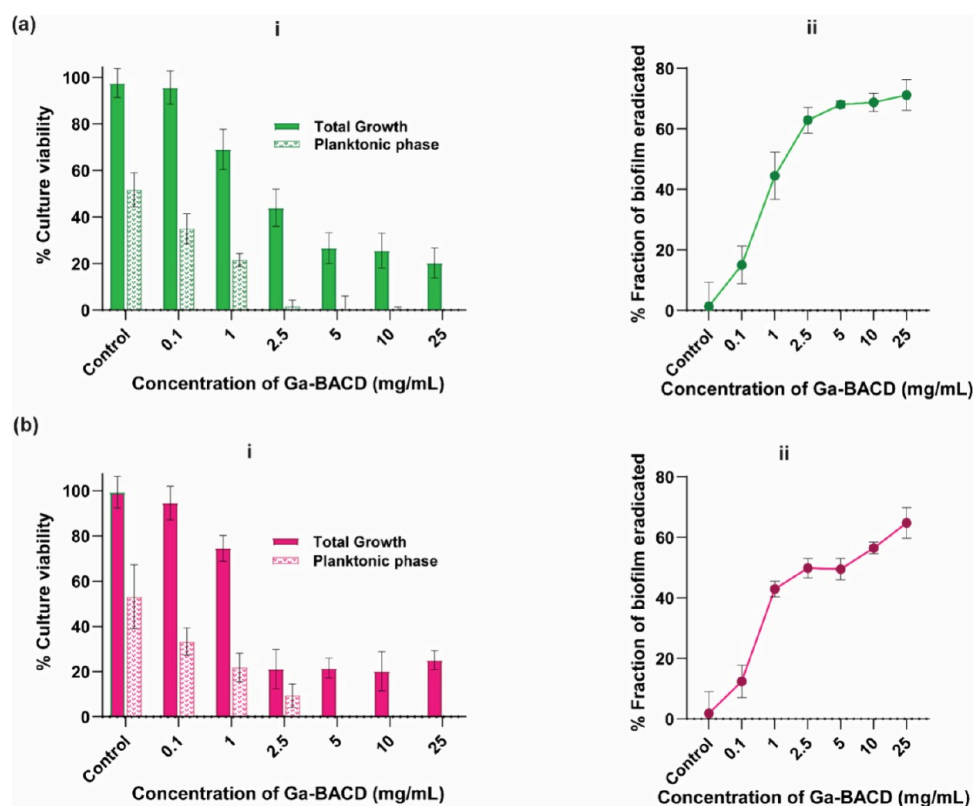


Figure 12. Biofilm eradication assay. The figure illustrates the eradication of mature biofilms of *Staphylococcus epidermidis* (SE) (a) and *E. coli* (b). Previously untreated biofilms were treated with Ga-BACDs and quantified total/planktonic growth (i) and biofilm (ii). Results represent the mean \pm SD values of triplicate readings from three different experiments.

were first incubated in a 96-well plate for 72 h to allow for the formation of a mature biofilm. Following incubation, the liquid phase, including planktonic bacteria, was carefully removed. The wells were then treated with varying concentrations of Ga-

BACDs (0–25 mg/mL) and incubated, after which total, planktonic (Figure 12a(i),b(i)), and biofilm-associated bacterial populations were quantified.

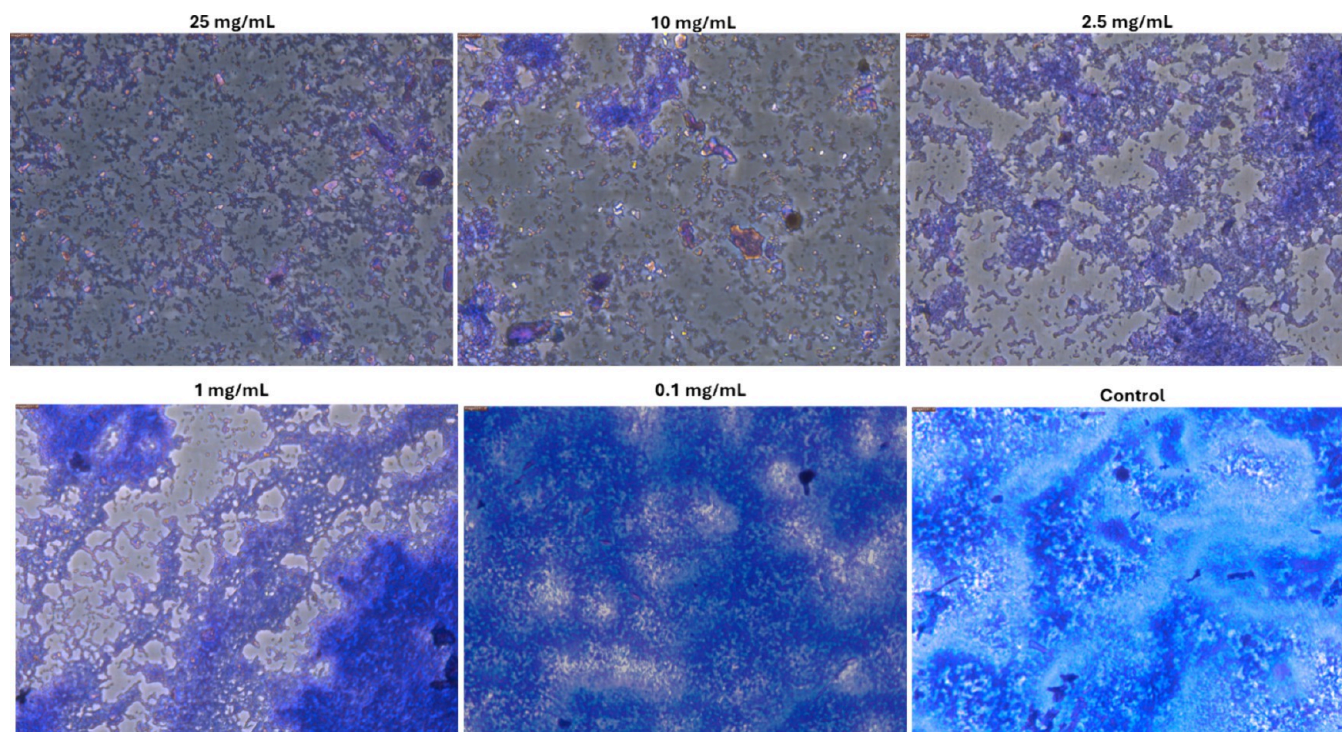


Figure 13. Biofilm eradication. Bright-field microscopy images of biofilm showing eradication of *Staphylococcus epidermidis* (SE biofilm) in the presence of increasing levels of Ga-BACDs. Significant disruption of biofilms was observed with Ga-BACDs at concentrations of ≥ 1 mg/mL.

At concentrations above 1 mg/mL, Ga-BACDs significantly disrupted preformed *Staphylococcus epidermidis* (SE) and *Escherichia coli* (*E. coli*) biofilms compared to untreated controls (Figure 12a(ii),b(ii)). This suggests that Ga-BACDs directly interact with bacteria within the established biofilm. Post-treatment analysis showed that, except at the lowest concentration (0.1 mg/mL), the number of viable bacteria within the biofilm was significantly reduced relative to control cells. The antibiofilm activity of Ga-BACDs may be attributed to multiple mechanisms, including direct particle–bacteria interactions that hinder bacterial adherence, interference with quorum sensing, and/or disruption of the extracellular matrix (ECM) integrity, which is crucial for biofilm stability.⁷³ This suggests that Ga-BACDs are effective against planktonic bacteria and target bacteria embedded within biofilms, which is a major challenge in treating chronic infections.

Bright-field microscopy further confirmed the eradication of *Staphylococcus epidermidis* (SE) (Figure 13) and *E. coli* biofilms (Figure S8). At concentrations of 2.5 mg/mL and above, planktonic bacterial growth was significantly inhibited with a 50% or more increase in biofilm eradicated. The percentage reduction in residual biofilm indicates that although Ga-BACD mainly acts on bacterial cells, it also interferes with components of the extracellular matrix, thereby hindering the development of new biofilms and breaking down established biofilm structures.

Our experimental studies have demonstrated that Ga-BACDs exhibit strong antibacterial activity and effective biofilm eradication, showing their potential as promising antimicrobial agents. These properties are particularly valuable in the context of biomedical applications, where biofilm-associated infections continue to pose serious clinical challenges.^{11,48} The data presented in this study support the feasibility of using Ga-BACDs as multifunctional agents capable of preventing bacterial colonization and biofilm formation. Based on our findings, the

study can be progressed toward application-specific studies, with a focus on medical implants, such as vascular stents and other implantable medical devices. These are high-risk areas where conventional treatments often fail due to the resistance of microbial biofilms and the limitations of systemic antibiotic therapy.⁷⁴

3.7. Cytotoxicity Studies on Ga-BACDs. The biocompatibility of BACDs was reported in our previous study.¹⁷ Consistent with those findings, Ga-BACDs also exhibited no *in vitro* toxicity at a 0.1 mg/mL concentration in a normal healthy human cell line (HBMEC), with 100% cell viability observed following treatment (Figure 14a). At a significantly higher concentration of Ga-BACDs (10 mg/mL), the cell survival was approximately $16.6 \pm 4.14\%$. Additionally, the cytotoxicity assay using Ga-BACD-coated paper discs ($255.7 \pm 47.8 \mu\text{g}/\text{mg}$) did not show any significant toxicity, with 99% cell viability observed (Figure 13 b). These results highlight the safety profile of Ga-BACD-coated surfaces for clinical applications.

4. CONCLUSIONS

In conclusion, this study demonstrates that the successful doping of gallium into phenylboronic acid carbon dots (Ga-BACDs), synthesized under optimized sonication conditions, exhibits enhanced optical and antibacterial properties compared with undoped BACDs. The Ga-BACDs exhibited superior antibacterial activity against Gram-negative *E. coli* and Gram-positive *Staphylococcus epidermidis*, significantly reducing bacterial viability. Additionally, Ga-BACDs effectively inhibited and eradicated bacterial biofilms, showcasing their potential as a promising tool for combating microbial infections. The Ga-BACDs also exhibited excellent biocompatibility in solutions, at 100 $\mu\text{g}/\text{mL}$ concentrations, and on cellulose surfaces, demonstrating significant potential for clinical applications,

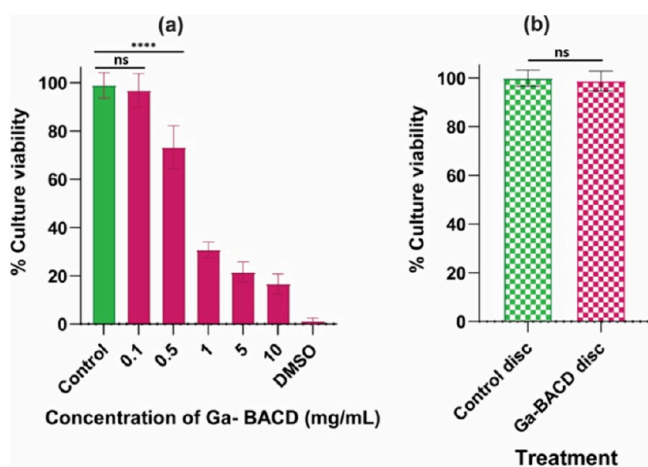


Figure 14. Toxicity assessment in human cell lines. The viability of human normal cell lines (HBMECs) was evaluated following exposure to CDs. Cell viability was assessed by an MTT assay, with results expressed as percentages and averaged over three independent experiments. (a) Viability test using Ga-BACD solutions at varying concentrations (0.1, 0.5, 1, 5, and 10 mg/mL). “Control” represents untreated cells, and “DMSO” denotes cells treated with DMSO as a positive control for cytotoxicity. (b) Biocompatibility test with paper discs. Human healthy cell lines were exposed to paper fibers coated with a 50 mg/mL CD solution, and cell viability was compared to that of untreated paper discs.

such as modifying medical implants and self-disinfecting surfaces.

■ ASSOCIATED CONTENT

SI Supporting Information

The Supporting Information is available free of charge at <https://pubs.acs.org/doi/10.1021/acsomega.5c03575>.

(Figure S1) Sonication setup for gallium doping on BACDs; (Figure S2) HR-SEM and EDX analysis on Ga-BACDs; (Figure S3) XRD deconvolution spectra; (Figure S4) antibacterial activity of BACD- and Ga-BACD-coated paper discs; (Figure S5) image showing the bacterial biofilm growth inhibition on a coverslip for the Ga-BACD-treated sample; (Figure S6) bright-field microscopy images showing inhibition of biofilm growth (*E. coli*); (Figure S7) 96-well plate layout showing biofilm growth inhibition in the presence of increasing levels of Ga-BACD, tested on a *Staphylococcus epidermidis* (SE) strain; (Figure S8) bright-field microscopy images of biofilm showing eradication of biofilm in the presence of increasing levels of Ga-BACDs (*E. coli*); (Figure S9) XPS survey spectra of BACDs and Ga-BACDs (PDF)

■ AUTHOR INFORMATION

Corresponding Author

Mohammad H. Al-Sayah – Department of Biology, Chemistry and Environmental Sciences, Materials Science and Engineering Program, College of Arts and Sciences, Materials Research Centre, College of Arts and Sciences, and Advanced Biosciences and Bioengineering Research Center, American University of Sharjah, Sharjah, United Arab Emirates; orcid.org/0000-0001-6321-0556; Email: malsayah@aus.edu

Authors

Remya Radha – Department of Biology, Chemistry and Environmental Sciences, American University of Sharjah, Sharjah, United Arab Emirates

Ahmad Fawad – Materials Science and Engineering Program, College of Arts and Sciences, American University of Sharjah, Sharjah, United Arab Emirates

Sreeshna Ravindran – Department of Biology, Chemistry and Environmental Sciences, American University of Sharjah, Sharjah, United Arab Emirates

Ganjaboy Boltaev – Materials Research Centre, College of Arts and Sciences, American University of Sharjah, Sharjah, United Arab Emirates

Sachin Philip – Department of Applied Chemistry, Cochin University of Science and Technology, Kochi, Kerala 682022, India

Complete contact information is available at:

<https://pubs.acs.org/10.1021/acsomega.5c03575>

Author Contributions

R.R.: Experiment design and conduction, draft layout, data collection, analysis of data, writing of the original draft, and manuscript editing; A.F.: data collection, experiment conduction, and writing; S.R.: antibacterial paper disc experiments; G.B.: HR-SEM experiments; S.P.: HR-TEM analysis; M.H.A.-S.: conceptualization, experiment design, guidance, funding acquisition, and draft editing.

Funding

We acknowledge the financial support of the American University of Sharjah through grant FRG24-C-S08.

Notes

All authors accepted final approval for publication and agreed for publication. We have not used AI-assisted technologies in creating this article.

The authors declare no competing financial interest.

■ ACKNOWLEDGMENTS

The authors acknowledge the technical and logistics support of the BCE Department and Office of Research at the American University of Sharjah, UAE. Authors acknowledge the Materials Research Center (MRC), American University of Sharjah for the experimental support for material characterizations. The authors acknowledge Dr. Fatin Samara, Professor at the College of Arts and Sciences, American University of Sharjah, for her instrumental support for microscopic analysis. We also express our gratitude to DST SAIF Kochi, India, for conducting the HR-TEM analysis.

■ REFERENCES

- (1) Muhammad, M. H.; Idris, A. L.; Fan, X.; Guo, Y.; Yu, Y.; Jin, X.; Qiu, J.; Guan, X.; Huang, T. Beyond Risk: Bacterial Biofilms and Their Regulating Approaches. *Front. Microbiol.* **2020**, *11*, No. 928.
- (2) Karygianni, L.; Ren, Z.; Koo, H.; Thurnheer, T. Biofilm Matrixome: Extracellular Components in Structured Microbial Communities. *Trends Microbiol.* **2020**, *28*, 668–681.
- (3) Funari, R.; Shen, A. Q. Detection and Characterization of Bacterial Biofilms and Biofilm-Based Sensors. *ACS Sens.* **2022**, *7*, 347–357.
- (4) Shree, P.; Singh, C. K.; Sodhi, K. K.; Surya, J. N.; Singh, D. K. Biofilms: Understanding the Structure and Contribution towards Bacterial Resistance in Antibiotics. *Med. Microecol.* **2023**, *16*, No. 100084.
- (5) Le Mauff, F.; Razvi, E.; Reichhardt, C.; Sivarajah, P.; Parsek, M. R.; Howell, P. L.; Sheppard, D. C. The Pel Polysaccharide Is

Predominantly Composed of a Dimeric Repeat of α -1,4 Linked Galactosamine and N-Acetylgalactosamine. *Commun. Biol.* **2022**, *5*, 502.

(6) Limoli, D. H.; Jones, C. J.; Wozniak, D. J. Bacterial Extracellular Polysaccharides in Biofilm Formation and Function. *Microbiol. Spectrum* **2015**, *3*, 3.3.29.

(7) Morales-García, A. L.; Walton, R.; Blakeman, J. T.; Banwart, S. A.; Harding, J. H.; Geoghegan, M.; Freeman, C. L.; Rolfe, S. A. The Role of Extracellular DNA in Microbial Attachment to Oxidized Silicon Surfaces in the Presence of Ca²⁺ and Na⁺. *Langmuir* **2021**, *37*, 9838–9850.

(8) Mirghani, R.; Saba, T.; Khaliq, H.; Mitchell, J.; Do, L.; Chambi, L.; Diaz, K.; Kennedy, T.; Alkassab, K.; Huynh, T.; et al. Biofilms: Formation, Drug Resistance and Alternatives to Conventional Approaches. *AIMS Microbiol.* **2022**, *8*, 239–277.

(9) Zhou, L.; Zhang, Y.; Ge, Y.; Zhu, X.; Pan, J. Regulatory Mechanisms and Promising Applications of Quorum Sensing-Inhibiting Agents in Control of Bacterial Biofilm Formation. *Front. Microbiol.* **2020**, *11*, No. 589640.

(10) Zarepour, A.; Venkateswaran, M. R.; Khosravi, A.; Irvani, S.; Zarrabi, A. Bioinspired Nanomaterials to Combat Microbial Biofilm and Pathogen Challenges: A Review. *ACS Appl. Nano Mater.* **2024**, *7*, 25287–25313.

(11) Mendhe, S.; Badge, A.; Ugemuge, S.; Chandi, D. Impact of Biofilms on Chronic Infections and Medical Challenges. *Cureus* **2023**, *15*, No. e48204.

(12) Omwenga, E. O.; Awuor, S. O. The Bacterial Biofilms: Formation, Impacts, and Possible Management Targets in the Healthcare System. *Can. J. Infect. Dis. Med. Microbiol.* **2024**, *2024*, No. 1542576.

(13) Vertes, A.; Hitchins, V.; Phillips, K. S. Analytical Challenges of Microbial Biofilms on Medical Devices. *Anal. Chem.* **2012**, *84*, 3858–3866.

(14) Kumar, L.; Bisen, M.; Harjai, K.; Chhibber, S.; Azizov, S.; Lalhlenmawia, H.; Kumar, D. Advances in Nanotechnology for Biofilm Inhibition. *ACS Omega* **2023**, *8*, 21391–21409.

(15) Mitra, A. Combatting Biofilm-Mediated Infections in Clinical Settings by Targeting Quorum Sensing. *Cell Surf.* **2024**, *12*, No. 100133.

(16) Gonzales, M.; Kergaravat, B.; Jacquet, P.; Billot, R.; Grizard, D.; Chabrière, É.; Plener, L.; Daudé, D. Disrupting Quorum Sensing as a Strategy to Inhibit Bacterial Virulence in Human, Animal, and Plant Pathogens. *Pathog. Dis.* **2024**, *82*, No. ftae009.

(17) Radha, R.; Makhlof, Z.; Diab, R.; Al-Sayah, M. H. Modifying Cellulose Fibres with Carbon Dots: A Promising Approach for the Development of Antimicrobial Fibres. *R. Soc. Open Sci.* **2024**, *11*, No. 231755.

(18) Ravindran, S.; Khan, D.; Khodja, A.; Terro, T.; Radha, R.; Diab, R.; Ialyshev, V.; Al-Sayah, M. H. Harnessing Piperine for Enhanced Antimicrobial Activity of Carbon Dot-Modified Cellulose Fibers. *Discovery Appl. Sci.* **2024**, *6*, 490.

(19) Li, Z.; Ye, B.; Fang, J.; Li, M.; Xiong, Y.; Xiong, P.; Zhou, Y.; Guo, Z.; Zhong, H.; Liu, Z. Engineering the Functional Surface of Carbon Dots for Antibacterial, Bacterial Bioimaging and Sensing Applications. *New J. Chem.* **2024**, *48*, 6020–6038.

(20) Hussien, N. H.; Hasan, A. H.; FaqiKhedr, Y. M.; Bogoyavlenskii, A.; Bhat, A. R.; Jamalis, J. Carbon Dot Based Carbon Nanoparticles as Potent Antimicrobial, Antiviral, and Anticancer Agents. *ACS Omega* **2024**, *9*, 9849–9864.

(21) Abraham, W. L.; Demirci, S.; Wypyski, M. S.; Ayyala, R. S.; Bhethanabotla, V. R.; Lawson, L. B.; Sahiner, N. Biofilm Inhibition and Bacterial Eradication by C-Dots Derived from Polyethyleneimine-Citric Acid. *Colloids Surf. B Biointerfaces* **2022**, *217*, No. 112704.

(22) Liu, M.; Huang, L.; Xu, X.; Wei, X.; Yang, X.; Li, X.; Wang, B.; Xu, Y.; Li, L.; Yang, Z. Copper Doped Carbon Dots for Addressing Bacterial Biofilm Formation, Wound Infection, and Tooth Staining. *ACS Nano* **2022**, *16*, 9479–9497.

(23) Priyadarshini, E.; Kumar, R.; Balakrishnan, K.; Pandit, S.; Kumar, R.; Jha, N. K.; Gupta, P. K. Biofilm Inhibition on Medical Devices and

Implants Using Carbon Dots: An Updated Review. *ACS Appl. Bio Mater.* **2024**, *7*, 2604–2619.

(24) Vijay, R.; Mendhi, J.; Prasad, K.; Xiao, Y.; Macleod, J.; Ostrikov, K.; Zhou, Y. Carbon Nanomaterials Modified Biomimetic Dental Implants for Diabetic Patients. *Nanomaterials* **2021**, *11*, No. 2977.

(25) Tasnim, N. T.; Ferdous, N.; Rumon, Md.M.H.; Shakil, M. S. The Promise of Metal-Doped Iron Oxide Nanoparticles as Antimicrobial Agent. *ACS Omega* **2024**, *9*, 16–32.

(26) Chandrakala, V.; Aruna, V.; Angajala, G. Review on Metal Nanoparticles as Nanocarriers: Current Challenges and Perspectives in Drug Delivery Systems. *Emergent Mater.* **2022**, *5*, 1593–1615.

(27) Shoudho, K. N.; Uddin, S.; Rumon, M. M. H.; Shakil, M. S. Influence of Physicochemical Properties of Iron Oxide Nanoparticles on Their Antibacterial Activity. *ACS Omega* **2024**, *9*, 33303–33334.

(28) Yaqoob, A. A.; Ahmad, H.; Parveen, T.; Ahmad, A.; Oves, M.; Ismail, I. M. I.; Qari, H. A.; Umar, K.; Mohamad Ibrahim, M. N. Recent Advances in Metal Decorated Nanomaterials and Their Various Biological Applications. *A Review. Front. Chem.* **2020**, *8*, No. 341.

(29) Luo, H.; Tuinenga, C.; Guidez, E. B.; Lewis, C.; Shipman, J.; Roy, S.; Aikens, C. M.; Chikan, V. Synthesis and Characterization of Gallium-Doped CdSe Quantum Dots. *J. Phys. Chem. C* **2015**, *119*, 10749–10757.

(30) Jeong, H.; Jo, S.; Yang, S.; Lee, S.; Surendran, S.; Nguyen, D. N.; Baek, U.; Kim, J. K.; Sim, U.; Shin, S. Determination of the Antibacterial Activity of Various Metal-Doped Carbon Quantum Dots. *Carbon Lett.* **2024**, *34*, 2183–2193.

(31) Najafu, M.; Shahgolzari, M.; Bani, F.; Khosroushahi, A. Y. Green Synthesis of Near-Infrared Copper-Doped Carbon Dots from Alcea for Cancer Photothermal Therapy. *ACS Omega* **2022**, *7*, 34573–34582.

(32) Wang, J.; Xu, M.; Wang, D.; Li, Z.; Primo, F. L.; Tedesco, A. C.; Bi, H. Copper-Doped Carbon Dots for Optical Bioimaging and Photodynamic Therapy. *Inorg. Chem.* **2019**, *58*, 13394–13402.

(33) Wang, Y.; Li, T.; Lin, L.; Wang, D.; Feng, L. Copper-Doped Cherry Blossom Carbon Dots with Peroxidase-like Activity for Antibacterial Applications. *RSC Adv.* **2024**, *14*, 27873–27882.

(34) Kumar, V. B.; Natan, M.; Jacobi, G.; Porat, Z.; Banin, E.; Gedanken, A. Ga@C-Dots as an Antibacterial Agent for the Eradication of *Pseudomonas Aeruginosa*. *Int. J. Nanomedicine* **2017**, *12*, 725–730.

(35) Qu, C.-C.; Liang, Y.-T.; Wang, X.-Q.; Gao, S.; He, Z.-Z.; Sun, X.-Y. Gallium-Based Liquid Metal Materials for Antimicrobial Applications. *Bioengineering* **2022**, *9*, No. 416.

(36) Li, F.; Liu, F.; Huang, K.; Yang, S. Advancement of Gallium and Gallium-Based Compounds as Antimicrobial Agents. *Front. Bioeng. Biotechnol.* **2022**, *10*, No. 827960.

(37) Limantorio, C.; Das, T.; He, M.; Dirin, D.; Manos, J.; Kovalenko, M. V.; Chrzanowski, W. Synthesis of Antimicrobial Gallium Nanoparticles Using the Hot Injection Method. *ACS Mater. Au* **2023**, *3*, 310–320.

(38) Chitambar, C. R. Gallium and Its Competing Roles with Iron in Biological Systems. *Biochim. Biophys. Acta BBA - Mol. Cell Res.* **2016**, *1863*, 2044–2053.

(39) Kaneko, Y.; Thoendel, M.; Olakanmi, O.; Britigan, B. E.; Singh, P. K. The Transition Metal Gallium Disrupts *Pseudomonas Aeruginosa* Iron Metabolism and Has Antimicrobial and Antibiofilm Activity. *J. Clin. Invest.* **2007**, *117*, 877–888.

(40) Song, G.; Li, M.; Zhou, B.; Qi, H.; Guo, J. Gallium-Based Metal-Organic Frameworks with Antibacterial and Anti-Inflammatory Properties for Oral Health Protection. *Heliyon* **2024**, *10*, No. e31788.

(41) Valappil, S. P.; Yiu, H. H. P.; Bouffier, L.; Hope, C. K.; Evans, G.; Claridge, J. B.; Higham, S. M.; Rosseinsky, M. J. Effect of Novel Antibacterial Gallium-Carboxymethyl Cellulose on *Pseudomonas Aeruginosa*. *Dalton Trans* **2013**, *42*, 1778–1786.

(42) Ramesh, G.; Kaviyil, J. E.; Paul, W.; Sasi, R.; Joseph, R. Gallium-Curcumin Nanoparticle Conjugates as an Antibacterial Agent against *Pseudomonas Aeruginosa*: Synthesis and Characterization. *ACS Omega* **2022**, *7*, 6795–6809.

(43) Kumar, V. B.; Perelshtein, I.; Lipovsky, A.; Porat, Z.; Gedanken, A. The Sonochemical Synthesis of Ga@C-Dots Particles. *RSC Adv.* **2015**, *5*, 25533–25540.

- (44) Sun, W.; Weingarten, R. A.; Xu, M.; Southall, N.; Dai, S.; Shinn, P.; Sanderson, P. E.; Williamson, P. R.; Frank, K. M.; Zheng, W. Rapid Antimicrobial Susceptibility Test for Identification of New Therapeutics and Drug Combinations against Multidrug-Resistant Bacteria. *Emerg. Microbes Infect.* **2016**, *5*, 1–11.
- (45) Abdullah, N. A.; Mahmoud, H. E.; El-Nikhely, N. A.; Hussein, A. A.; El-Khordagui, L. K. Carbon Dots Labeled Lactiplantibacillus Plantarum: A Fluorescent Multifunctional Biocarrier for Anticancer Drug Delivery. *Front. Bioeng. Biotechnol.* **2023**, *11*, No. 1166094.
- (46) Radha, R.; Paul, V.; Anjum, S.; Bouakaz, A.; Pitt, W. G.; Hussein, G. A. Enhancing Curcumin's Therapeutic Potential in Cancer Treatment through Ultrasound Mediated Liposomal Delivery. *Sci. Rep.* **2024**, *14*, 10499.
- (47) Kaur, H.; Sareen, S.; Verma, M.; Vashisht, A.; Sharma, A.; Kataria, R.; Mehta, S. K.; Park, J.; Mutreja, V. Effect of Synthesis Methods and Conditions on Properties and Applications of Carbon Dots for the Detection of Potential Water Contaminants: A Review. *Crit. Rev. Anal. Chem.* **2023**, *53*, 751–774.
- (48) Selvaraju, N.; Ganesh, P. S.; Palrasu, V.; Venugopal, G.; Mariappan, V. Evaluation of Antimicrobial and Antibiofilm Activity of Citrus Medica Fruit Juice Based Carbon Dots against *Pseudomonas Aeruginosa*. *ACS Omega* **2022**, *7*, 36227–36234.
- (49) Sun, H.; Sun, S.; Wang, H.; Cheng, K.; Zhou, Y.; Wang, X.; Gao, S.; Mo, J.; Li, S.; Lin, H.; et al. Phenylboronic Acid-Modified Carbon Dot-Proteinase K Nanohybrids for Enhanced Photodynamic Therapy against Bacterial Biofilm Infections. *Acta Biomater.* **2025**, *194*, 352–363.
- (50) Mosina, M.; Kovrlija, I.; Stipniece, L.; Locs, J. Gallium Containing Calcium Phosphates: Potential Antibacterial Agents or Fictitious Truth. *Acta Biomater.* **2022**, *150*, 48–57.
- (51) Quan, Y.; Fang, D.; Zhang, X.; Liu, S.; Huang, K. Synthesis and Characterization of Gallium Oxide Nanowires via a Hydrothermal Method. *Mater. Chem. Phys.* **2010**, *121*, 142–146.
- (52) Rambabu, U.; Munirathnam, N. R.; Prakash, T. L.; Vengalrao, B.; Buddhudu, S. Synthesis and Characterization of Morphologically Different High Purity Gallium Oxide Nanopowders. *J. Mater. Sci.* **2007**, *42*, 9262–9266.
- (53) Gao, X.; Yu, H.; Han, Z.; Chen, B.; Sun, J.; Li, X. Bright Solid-State Luminescence and High-Temperature Resistance of Ga-Doped Carbon Dots with Ultra-Wideband White Emission for Light-Emitting Diodes. *Dalton Trans.* **2023**, *52*, 16388–16397.
- (54) Parveen, K.; Rafique, U.; Akhtar, M. J.; Ashokumar, M. Ultrasound-Assisted Synthesis of Gallium Hybrids for Environmental Remediation Application. *Ultrason. Sonochem.* **2018**, *49*, 222–232.
- (55) Pochapski, D. J.; Carvalho Dos Santos, C.; Leite, G. W.; Pulcinelli, S. H.; Santilli, C. V. Zeta Potential and Colloidal Stability Predictions for Inorganic Nanoparticle Dispersions: Effects of Experimental Conditions and Electrokinetic Models on the Interpretation of Results. *Langmuir* **2021**, *37*, 13379–13389.
- (56) Nissan, I.; Kumar, V. B.; Porat, Z.; Makovec, D.; Shefi, O.; Gedanken, A. Sonochemically-Fabricated Ga@C-dots@Ga Nanoparticle-Aided Neural Growth. *J. Mater. Chem. B* **2017**, *5*, 1371–1379.
- (57) Hu, S.-L.; Niu, K.-Y.; Sun, J.; Yang, J.; Zhao, N.-Q.; Du, X.-W. One-Step Synthesis of Fluorescent Carbon Nanoparticles by Laser Irradiation. *J. Mater. Chem.* **2009**, *19*, 484–488.
- (58) Li, H.; Kang, Z.; Liu, Y.; Lee, S.-T. Carbon Nanodots: Synthesis, Properties and Applications. *J. Mater. Chem.* **2012**, *22*, 24230.
- (59) Zhang, Y.; Park, M.; Kim, H. Y.; Ding, B.; Park, S.-J. A Facile Ultrasonic-Assisted Fabrication of Nitrogen-Doped Carbon Dots/BiOBr up-Conversion Nanocomposites for Visible Light Photocatalytic Enhancements. *Sci. Rep.* **2017**, *7*, No. 45086.
- (60) Lu, M.; Zhou, L. One-Step Sonochemical Synthesis of Versatile Nitrogen-Doped Carbon Quantum Dots for Sensitive Detection of Fe²⁺ Ions and Temperature in Vitro. *Mater. Sci. Eng., C* **2019**, *101*, 352–359.
- (61) Kumar, R.; Kumar, V. B.; Gedanken, A. Sonochemical Synthesis of Carbon Dots, Mechanism, Effect of Parameters, and Catalytic, Energy, Biomedical and Tissue Engineering Applications. *Ultrason. Sonochem.* **2020**, *64*, No. 105009.
- (62) Lin, H.; Ding, L.; Zhang, B.; Huang, J. Detection of Nitrite Based on Fluorescent Carbon Dots by the Hydrothermal Method with Folic Acid. *R. Soc. Open Sci.* **2018**, *5*, No. 172149.
- (63) Fajarwati, F. I.; Hidayat, R.; Fadillah, G. Synthesis and Transformation of Graphene-like Structures from Bamboo Waste for Photoelectrochemical Devices. *Carbon Trends* **2024**, *15*, No. 100351.
- (64) Li, Z.; Deng, L.; Kinloch, I. A.; Young, R. J. Raman Spectroscopy of Carbon Materials and Their Composites: Graphene. *Nanotubes and Fibres. Prog. Mater. Sci.* **2023**, *135*, No. 101089.
- (65) Lee, J.; Kim, T.; Ryu, S. U.; Choi, K.; Ahn, G. H.; Paik, J. G.; Ryu, B.; Park, T.; Won, Y. S. Study on the Aging Mechanism of Boron Potassium Nitrate (BKNO₃) for Sustainable Efficiency in Pyrotechnic Mechanical Devices. *Sci. Rep.* **2018**, *8*, 11745.
- (66) Moulder, J. F.; Chastain, J. *Handbook of X-Ray Photoelectron Spectroscopy: A Reference Book of Standard Spectra for Identification and Interpretation of XPS Data*; Physical Electronics Division, Perkin-Elmer Corporation, 1992; ISBN 978–0-9627026–2-4.
- (67) Ong, C. W.; Huang, H.; Zheng, B.; Kwok, R. W. M.; Hui, Y. Y.; Lau, W. M. X-Ray Photoemission Spectroscopy of Nonmetallic Materials: Electronic Structures of Boron and BxOy. *J. Appl. Phys.* **2004**, *95*, 3527–3534.
- (68) Ghosh, S. C.; Biesinger, M. C.; LaPierre, R. R.; Kruse, P. X-Ray Photoelectron Spectroscopic Study of the Formation of Catalytic Gold Nanoparticles on Ultraviolet-Ozone Oxidized GaAs(100) Substrates. *J. Appl. Phys.* **2007**, *101*, 114322.
- (69) Singh, S.; Datta, S.; Narayanan, K. B.; Rajnish, K. N. Bacterial Exo-Polysaccharides in Biofilms: Role in Antimicrobial Resistance and Treatments. *J. Genet. Eng. Biotechnol.* **2021**, *19*, 140.
- (70) Al Awak, M. M.; Wang, P.; Wang, S.; Tang, Y.; Sun, Y.-P.; Yang, L. Correlation of Carbon Dots' Light-Activated Antimicrobial Activities and Fluorescence Quantum Yield. *RSC Adv.* **2017**, *7*, 30177–30184.
- (71) Shi, F.; Ma, S.; Liu, S.; Xin, R.; Chen, B.; Ye, W.; Sun, J. A Novel Antimicrobial Strategy for Bacterial Infections: Gallium-Based Materials. *Colloid Interface Sci. Commun.* **2023**, *56*, No. 100735.
- (72) Lin, F.; Li, C.; Chen, Z. Bacteria-Derived Carbon Dots Inhibit Biofilm Formation of *Escherichia Coli* without Affecting Cell Growth. *Front. Microbiol.* **2018**, *9*, No. 259.
- (73) Roy, R.; Tiwari, M.; Donelli, G.; Tiwari, V. Strategies for Combating Bacterial Biofilms: A Focus on Anti-Biofilm Agents and Their Mechanisms of Action. *Virulence* **2018**, *9*, 522–554.
- (74) Nahum, Y.; Muhvich, J.; Morones-Ramirez, J. R.; Casillas-Vega, N. G.; Zaman, M. H. Biofilms as Potential Reservoirs of Antimicrobial Resistance in Vulnerable Settings. *Front. Public Health* **2025**, *13*, No. 1568463.